Design of hierarchical architectures in metal-organic frameworks for catalysis and adsorption

Francisco G. Cirujano[a]*, Nuria Martin[a] and Lik H. Wee[b]*

F. G. Cirujano and N. Martín

Instituto de Ciencia Molecular (ICMol), Universitat de València, Catedrático José Beltrán Martínez nº 2, 46980 Paterna, Valencia, Spain
E-mail: francisco.c.garcia@uv.es

L. H. Wee

Department of Chemical Engineering & Biotechnology, University of Cambridge, Philippa Fawcett Drive, Cambridge, CB3 0AS UK

E-mail: lhw31@cam.ac.uk

KEYWORDS Hierarchical, Mesoporous, MOFs, Adsorption, Catalysis

ABSTRACT: A key factor to improve the performance of metal-organic frameworks (MOFs) is the design and synthesis of hierarchical interconnected porosity at different length scales. The presence of secondary mesopore systems, in addition to the intrinsic framework micropores, avoids inherent mass-transfer constraints that occur in multiple examples of liquid phase chemical processes. Different strategies to introduce ordered void spaces in the MOF materials are reviewed here, based on either bottom-up or top-down approaches. A thorough discussion of the different bottom-up synthesis protocols, based on the interactions of the molecular building blocks with soft or hard templates, is followed by presenting synthesis concepts relating to multi-dimensional MOF transformations, interfacial and modulated synthesis. The holy grail of defect engineering MOF crystals with controlled porosity is tackled through several top-down approaches in the nanoscale regime. The resultant hierarchical MOFs with interconnected porosity represent the next generation of advanced catalysts and adsorbents, as is presented here by using a vast number of examples where the hierarchical porous structure is key to the MOF performance. A combination of tailor-made pore shape, size and functionality, leads to a synergistic effect between the MOF structures and functions, which offers an improvement on catalysis and adsorption while preserving their porosity, reactivity and stability. The hierarchical MOFs presented in the different sections of this review are compared with the purely microporous parent MOFs, used as benchmark in challenging applications where the performance is boosted in the case of hierarchical MOFs.

1. Introduction

Crystalline materials with hierarchical porous architectures have well defined structures at the atomic scale, presenting different interconnected pore systems on multiple length scales from micro (<2 nm) to meso (2-50 nm) and even macroporous (>50nm).[1, 2] The active sites present in a porous solid are often confined in their micropores, which can impose severe intrinsic mass-transfer constraints in catalytic and adsorptive related processes in the liquid phase. Restricted molecular access and slow diffusivity of the substrates/products to/from the active site (mass transport limitations) have often resulted in lower catalytic performance, i.e. coke formation. For instance, in liquid phase zeolite catalysis, transport limitations severely affect not only its catalytic activity but also its selectivity and lifetime stability of the microporous zeolite catalyst. In this sense, the mass transport limitations are solved by (i) introducing a secondary mesopore system in the microporous solid; and/or (ii) shortening the micropore diffusion path length via scaling down the crystal size to the nanoscale regime. Thus, the synthesis of hierarchical and nanosized zeolites for improving their catalytic performance has become one of the major trends in zeolite and zeotype related research over the last decades.[3-13]

The concept of reticular synthesis has been employed to assemble metal-organic frameworks (MOFs) from molecular building blocks (secondary building units). This particular type of crystalline nanoporous solids, constituted of metal ions/clusters bonded to multidentate organic molecules (also known as linkers) through coordination bonds, has become one of the fastest growing fields in chemistry.[14-16] MOFs have long-range ordered crystalline structures with pore sizes between several angstroms and few nanometers,

determined by the primary building units or molecular building blocks. To date, the vast majority of the reported MOFs have only micropores in their crystalline networks, thus limiting the catalytic applications to the transformation of small substrates.[17-19] The synthesis of hierarchical MOFs with mesostructures is limited by the classical solvothermal synthesis technique where metal salts and short length organic linkers are employed. Hierarchical MOFs with interconnected porosity at different length scales are of relevance for optimizing their catalytic performance and adsorption processes. This is due to the favored accessibility of the inner active sites located inside the porous structures.

In this review, we summarize the recent advances in the design and synthesis of MOFs with hierarchical porosity across the micro- and mesoporous regimes through either bottom-up or top-down strategies. The first one focuses on the design of the different types of molecular building blocks of the MOF, additives or growth modulators and their particular self-assembly under the optimal synthetic conditions. The aim of the latter is the rational manipulation of the MOF crystal, with atomic precision, in expanding the pore cavity from the micro- to the meso- and even macrodomain. For each category, detailed MOF synthesis examples are illustrated and their enhanced properties (arising from the hierarchically interconnected micro- and mesoporosities present in the porous networks) evaluated in catalysis and adsorption related applications.

We divide this review into seven sections, with the first section being the introduction and the last section the conclusions and outlook of the field. The sections in between demonstrate different protocols adopted to create a hierarchical pore system in MOFs (**Table 1**). The information consists of a summary covering their structural properties such as BET area, pore volume, topology, pore size and applications in catalysis, gas storage and adsorptive separation. In section 2, we start with the design and combination of secondary building units, another term for molecular building blocks, as a unique and precise bottom-up approach for the synthesis of classic mesoporous MOFs, such as Cr-MIL-101 (section 2.1). We provide an overview of this mesoporous MOF as a platform for further post-synthetic chemical modification as well as a host for the encapsulation of polyoxometalates and nanoparticles, among others. Next, the use of extended linkers (section 2.2), mixed-linker (section 2.3), modulator-induced defect engineering (section 2.4) and 1D-2D-3D topotactic transformation synthesis (section 2.5) are discussed based on recent examples from literature. In section 3, we summarize the synthesis of hierarchical MOFs assisted by soft templates such as ionic surfactants (section 3.1), non-ionic surfactants (section 3.2) and hydrogels (section 3.3). Then, the implementation of polymers such as polystyrene spheres (section 4.1), metal nanoparticles (section 4.2) and metal-organic polyhedra (section 4.3) as hard templates for the generation of hierarchical pore structures are revised in section 4. Secondary mesoporosity referring to interparticle voids formed via stacking of nanocrystalline MOFs is highlighted in section 5. We describe the top-down engineering of hierarchical MOFs in section 6, where acid leaching (section 6.1) and linker labilization with temperature or light (sections 6.2 and 6.3) appear to be efficient alternative approaches for the generation of secondary mesoporosity in microporous MOFs. This review ends with conclusions and a future outlook to guide the reader on the possible directions of the field in the near future (section 7).

2. Bottom-up engineering of mesoporous MOFs

2.1. Secondary building units (SBU)

SBUs are described as pre-designed topology of the MOF nodes which are made of several oligonuclear metal-oxo/aza containing building blocks, depending on the nature of the linker. These well-defined SBUs are then assembled into predetermined ordered structures or networks by strong coordination bonding of metal ions and functional groups of organic linkers via reticular "self-assembled" synthesis. The combination of reticular chemistry and computational simulations has been applied by Ferey and coworkers for the design of hierarchical MOFs with large mesopores such as MIL-101(Cr) and MIL-100(Cr) (MIL = Material Institute Lavoisier) which exhibit large mesopores interconnected through smaller micropore windows (entries 1 and 2 of Table 1).[20, 21] This strategy only uses simple and short linkers, such as benzenetricarboxylate (BTC) or terephthalate (BDC) ligands, which is often the case for the synthesis of well-studied HKUST-1 (HKUST= Hong Kong University of Science and Technology), MOF-5, UiO-66-type microporous MOFs. The synthesis of MIL-101, from BDC linkers and inorganic μ_3-oxo bridged trimeric Cr_3O octahedral building units, forms a 3D network with MTN zeotype architecture. The resulting giant framework possesses one mesoporous cage with ~29 Å and another with 34 Å diameters composed from 20 and 28 super tetrahedrons, respectively (**Figure 1**). These large windows of both cages are interconnected through smaller microporous cages with micropore windows of ~12, 14.5 and 16 Å. However, it shall be noted that the implication of this synthesis concept for the engineering of other mesoporous MOFs remains a great challenge. For the interested reader, the application of MIL-101 for adsorption and catalysis has been thoroughly reviewed.[22, 23]

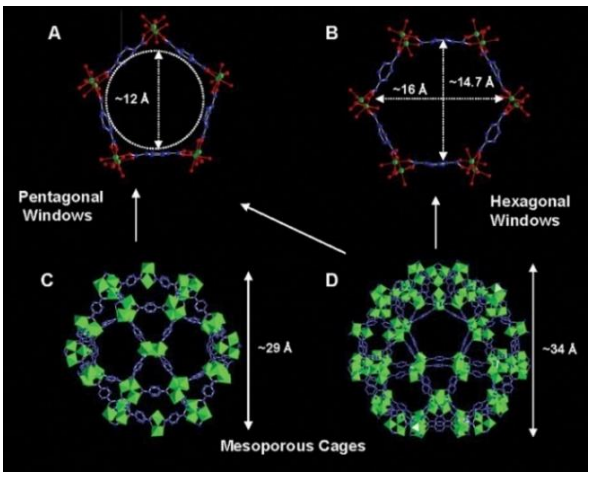

Figure 1. Structure of MIL-101 mesoporous MOF indicating the cavity and type of windows to access. Reproduced with permission.[20] Copyright 2004, Wiley.

Table 1. Representative hierarchical/mesoporous MOFs and their structural features.

	Hierarchical/ Mesoporous MOF	Method	Surface area ($m^2\ g^{-1}$)	Pore volume ($cm^3\ g^{-1}$)	Micropore size /nm	Mesopore size/nm	Topology	Ref.
1	Cr-MIL-101	SBU	4100	2.0	1.2, 1.47, 1.6	2.9, 3.4	MTN	20
2	Cr-MIL-100	SBU	2800	1.16	0.66	2.5, 2.9	MTN	21
3	NU-1000	Extended linker	2320	1.4	1.2	3.0	csq	43
4	NU-1003	Extended linker	2300	1.5	12 × 13	2.3, 4.7	csq	48
5	NU-1004	Extended linker	2500	1.6	14 × 16	2.6, 5.1	csq	48
6	NU-1005	Extended linker	2600	1.7	17 × 19	3.0, 6.0	csq	48
7	NU-1006	Extended linker	3100	1.8	1.8 × 2.0	3.1, 6.2	csq	48
8	NU-1007	Extended linker	2700	2.3	-	2.2 × 2.4, 3.3, 6.7	csq	48
9	PCN-600	Extended linker	2270	1.8	-	3.1	stp-a	49
10	PCN-222	Extended linker	2200[a]	1.56	-	3.7	Kagome	50
11	PCN-228	Extended linker	4510	-	-	2.5	ftw-a	51
12	PCN-229	Extended linker	4619[j]	-	-	2.8	ftw-a	51
13	PCN-300	Extended linker	4455	-	-	3.8	ftw-a	51
14	NDISA	Extended linker	1722	-	-	3.3	etb	53
15	MIT-25	Extended linker	330	-	0.5 × 0.56	2.64 × 3.05	ssp	54
16	DUT-46	Extended linker	2704	2.29	1.08; 1.49	4.3	fcu	55
17	DUT-49	Extended linker	5479	2.81	1.2; 1.8	2.6	fcu	57
18	DUT-50	Extended linker	4620	3.41	1.08	2.1; 3.07	fcu	55
19	DUT-151	Extended linker	4841	4.43	1.08	2.4; 3.49	fcu	55
20	Zn_2(dobpdc)	Extended linker	3440	-	-	2.2	etb	60
21	PCN-777	Extended linker	2008	2.8	-	3.8	β - cristobalite	61
22	ZnBDP	Extended linker	2200	0.71	1.32	-	$P4_2/mmc$	63
23	MIT-20	Extended linker	2066	-	-	2.3	mer	66
24	UMCM-1	Mixed-linker	4160	-	1.4 × 1.7	2.7 × 3.2	muo	70
25	UMCM-2	Mixed-linker	5200	-	1.4-1.6; 1.6-1.8	2.4-3.0	umt	71
26	DUT-6	Mixed-linker	6411	3.16	-	2.5-3.0	lth-d	76
27	DUT-32	Mixed-linker	838	2.91	1.4 × 1.8	3 × 4; 2.8 × 3.2; 2 × 2.6	umt	77
28	MOF-210	Mixed-linker	6240	3.60	-	2.69 × 4.83	toz	78
29	DUT-60	Mixed-linker	7839	5.03	-	1.5 × 2.7; 3.7 × 4.2	lth-d	79
30	PCN-125	Modulator induced defect engineering	1210	-	1.0	5.8	nbo	94

31	COK-18	Topotactic trans-formation	800	0.45	1.1	12	-	107
32	HKUST-1	Polymer	527	0.3	0.5; 1.0; 1.35	4-12	tbo	125
		Stacking of nanoparticles	612-1048	0.82-1.12	0.5; 1.0; 1.35	26-72	tbo	135
		Stacking of nanoparticles	700	1.28	0.5; 1.0; 1.35	12-23	tbo	136
33	HZIF-67	Hydrogel	1483	0.71	-	16-27	sod	126
		PVP	1654	0.12	-	20-40		128
34	MOF-74	Stacking of nanoparticles	236-638	0.24-0.49	1.1	5-20	etb	137
		Stacking of nanoparticles	402-1007	0.27-1.04	-	2.4-29.3	etb	138
35	UiO-66	Stacking of nanoparticles	1459	2.09	0.6; 0.8	15	fcu	143
		Acid leaching	980	0.72	1.5	5.5	fcu	93
		Thermolysis	1022	-	1.5	9.8	fcu; reo	151
		Photolysis	-	-	-	3.0	-	153
36	UiO-67	Thermolysis	2185	-	-	14.8	-	151
		Photolysis	2008	-	-	2.3	-	153
37	MIL-121	Thermolysis	479	1.01	-	6.8	-	151
38	POST-66	Hydrolysis	620	0.94	-	3.8; 13.9	reo	154

Thus, in the present review, we will only highlight recently published works on MIL-101 type MOF for adsorptive and catalytic processes. For instance, Cr-MIL-101, and its ethylenediamine (ED), diethylenetriamine (DETA) and N-(phosphonomethyl)iminodiacetic acid (PMIDA) functionalized derivatives have been reported to be efficient adsorbents of rare earth elements (such as La^{3+}, Ce^{3+}, Nd^{3+}, Sm^{3+}, and Gd^{3+}) from aqueous solutions, showing great potential for their industrial separation and recovery.[24] Remarkably, MIL-101-PMIDA material adsorbed the highest amount of Gd^{3+} (87.7 mg·g^{-1}), over a wide pH range (pH 3-6) at 25 °C, via electrostatic interactions with the organic functions (e.g. free amines and hydroxyl groups) grafted on MIL-101, followed by MIL-101-DETA (73.6 mg g^{-1}), MIL-101-ED (66 mg g^{-1}), MIL-101-NH_2 (29.3 mg g^{-1}) and MIL-101 (16.5 mg g^{-1}). Besides inorganic species, basic quinoline and neutral indole compounds have been adsorbed from n-octane over the protonated polyaniline incorporated in MIL-101, reaching 556 and 602 mg·g^{-1} of uptake, respectively.[25]

MIL-101 has been recently documented as an active, selective and stable catalyst for promoting the benzylic oxidation of hydrocarbons. For instance, MIL-101 catalyst showed high selectivity towards the production of indanol and indanone when indane was used as a substrate, with a selectivity of 87% at 30% conversion.[26] It should be noted that no additional oxidizing agents nor initiator is required to promote the reaction. MIL-101 is also an ideal host material of heteropolyacids or polyoxometalates (HPAs or POMs) due to their (i) large size mesocages for uniform dispersion and high loading of HPAs up to 50 wt%, (iii) extraordinary surface area, (iv) simple and fast synthetic procedures employing terephthalic acid as a linker and (v) robustness with respect to other MOF-type materials. The synergistic effects of the encapsulated HPAs in the cavities of MIL-101 enhance the Brønsted acidity as well as the overall framework stability of the host. These MIL-101(HPAs) MOF materials have shown promising catalytic activity and recoverability for a vast range of fine chemical synthesis.[27-33] Previous contributions studied the different strategies for POMs immobilization within MOF structures as a host for fine chemical synthesis.[27] For instance, phosphotungstic acid encapsulated on Cr-MIL-101 has been demonstrated to be a high performant heterogeneous catalyst for the selective ring opening of styrene oxide with methanol with 99% yield.[32] MIL-100 catalyst also showed superior selectivity for catalyzing the self-condensation of cyclopenanone or cyclohexanone.[33] Selectivity of 2-cyclopentylidenecyclopentanone up to 98% was achieved from the self-condensation of cyclopentanone in 48 h at 130 °C. After hydrodeoxygenation, the reaction products have a density of 0.867 g·ml^{-1}, which confirmed the applicability of MIL-101 as a promising heterogeneous catalyst towards high-density biofuels from biomass valorization.

The large surface area of MIL-101(Cr) makes it also an ideal matrix for the uniform encapsulation of nanoparticles and inorganic functional compounds. For example, MIL-101 has been used as a host for the homogeneous dispersion and growth of CdS coated Au nanoparticles. The resulting Au@CdS/MIL-101 heterostructure exhibited a superior hydrogen evolution rate of 250 μmol·h^{-1} under visible light irradiation, which is 2.6 times higher than that of pure CdS, obtained from water splitting.[34] In another study, the Pd nanoparticles incorporated in Ce-doped MlL-101 generated 495 μmol of ammonia borane derived H_2 under visible light irradiation after one hour. This resulted in a TurnOver-Number (TON) of 2357.[35] In the presence of electron-rich Pd nanoparticles, the resulting Pd/CeMlL-101 mesoporous MOF exhibited synergic effects due to (i) the facilitated photo-generated charge separation on (Ce^{4+}/Ce^{3+}) redox pair and (ii) the generation of hydroxyl radicals and superoxide anions.

Tsapatsis and co-workers reported the one-pot synthesis of MIL-101 with incorporated chromium hydroxide within its porous structure.[36] This type of MOF base-contained material is highly selective for the conversion of glucose to fructose in the presence of ethanol, with comparable catalytic performance to benchmark Sn-Beta zeolite catalyst. Remarkably, the fructose yield on $Cr(OH)_3$@MIL101 was 59% at 76% fructose conversion after 24 h at 100 °C. Interestingly, NMR spectroscopy studies with isotopically labeled molecules confirmed that the isomerization of glucose to fructose on this catalyst is initiated predominantly via a proton-transfer mechanism, which is different from what has been reported for Sn-Beta catalyst, where the isomerization of glucose to fructose is achieved via intramolecular hydride shift mechanism.

Aiming at the valorization of biomass derived fructose, De Vos and co-workers reported the use of highly defective UiO-66-NH_2 MOF as heterogeneous catalysts for the fructose dehydration into hydroxymethylfurfural (HMF).[37] The pore size distributions of the -NH_2 containing MOF indicated large pores at ~1.5 nm, beside those at ~0.6 nm (for the less defective NO_2 containing MOFs) suggesting that not only linkers but also clusters may be missing. This was confirmed by the low-angle (2θ = 1-10º) region (reo nanoregions) of the PXRD patterns of the MOFs, indicating a decrease of the reflection at 4º upon increasing nitro-linker content, which suggest the decrease of domains with reo topology. This resulted in a more open framework, since both surface area and pore volume increases twofold in UiO-66-NH_2 (S_{area} = 811 $m^2 \cdot g^{-1}$, V_{pore} = 0.47 $cm^3 \cdot g^{-1}$) with respect to UiO-66-NO_2 (S_{area} = 422 $m^2 \cdot g^{-1}$, V_{pore} = 0.25 $cm^3 \cdot g^{-1}$). Thus, the access of fructose to the catalytic active sites and the yield of HMF improved from 47% (for pure UiO-66-NO_2) to 71% (for pure UiO-66-NH_2) after 1 h.

Recently, Roman-Leshkov and co-workers reported the preparation $Co(CO)_4^-$-incorporated Cr-MIL-101 as heterogeneous catalyst for the ring-expansion-carbonylation of epoxides.[38] The catalytic performance of $Co(CO)_4$@Cr-MIL-101 is comparable to reported homogeneous catalysts, such as $[(cyclopentadienyl)_2Ti(THF)_2]^+[Co(CO)_4]^-$ and [(N,N′-o-phenylenebis(3,5-di-tertbutylsalicylideneimine)$Al(THF)_2]^+$ $[Co(CO)_4]^-$, under similar reaction conditions. For instance, when 1,2-epoxyhexane was used as a substrate, $Co(CO)_4$@Cr-MIL101 catalyst produced the corresponding β-lactone in up to 86% yield. The calculated space-time yield was 34 h^{-1}, in line with state-of-the-art homogeneous catalysts.

2.2 Extended linkers for the synthesis of mesoporous MOFs

By increasing the length of the linkers, i.e. adding more aromatic rings between the coordinating functional groups (**Scheme 1**), the porosity of the final solid MOF can be extended into the mesopore scale with pore diameter ranges from 2–50 nm.[39, 40] However, most of the synthesis methods described to prepare large linkers require expensive reagents and tedious procedures and the final MOFs obtained tend to possess poor stability with respect to shorter linkers, such as benzene-1,4-dicarboxylic acid (BDC). Moreover, the use of extended linkers for mesoporous MOF synthesis often leads to undesirable structural collapse or framework catenation upon removal of the solvent molecules, e.g. trapped DMF in the pores. This would drastically reduce the pore size and porosity (free volume), limiting its catalytic and adsorptive performances.[41, 42] Nonetheless, isoreticular pore expansion enables one to synthesize MOFs with tunable pore sizes.

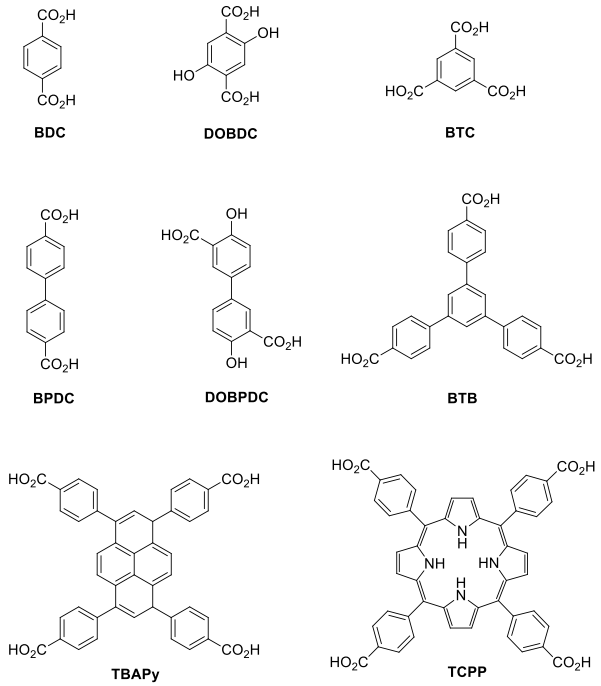

Scheme 1. Extended linkers employed as building blocks of mesoporous MOFs.

In this section, we would like to highlight a few recent advances in the design of extended linkers and their use to construct MOFs with ultra-large mesopores and high permanent porosities. One of such examples is a robust Zr-based 1,3,6,8-tetrakis(p-benzoate)pyrene (TBAPy) mesoporous MOF termed as NU-1000 with interconnected microporous structure was successfully synthesized by Farha's group, based on the csq-net design concept (**Figure 2**).[43, 44] The one-dimensional pores of crystalline NU-1000 with a mesopore size of ~ 3.0 nm and a micropore size of ~1.2 nm (entry 3 of Table 1) are capable of encapsulating insulin molecules (kinetic diameter = 1.3 × 1.3 nm) in up to ~40 wt% loading after only 30 min via electrostatic and/or

hydrophobic interactions. The demonstrated concept also helps to prevent insulin degradation from stomach acid and the digestive enzyme pepsin (size 4.8 × 6.4 nm), thereby limiting its proteolysis.[45, 46] The large mesopores of NU-1000 are also suited to encapsulate *Fusarium solani pisi cutinase* (PDB: 1CEX), a biocatalyst that promotes the hydrolysis of *p*-nitrophenyl butyrate to produce aliphatic esters. Cutinase@NU-1000 showed comparable catalytic performance to the free cutinase under a similar buffer system. More importantly, NU-1000 was an excellent host for stabilizing the encapsulated cutinase enzyme in different backgrounds such as THF and urea, where the free enzymes would have been degraded immediately under similar conditions. This work inspired further work on MOF biocomposites for catalytic applications.[47]

The same group has successfully designed a new series of mesoporous csq-net Zr-MOFs denoted as NU-1003, NU-1004, NU-1005, NU-1006 and NU-1007 with even larger mesopore sizes and pore volumes than NU-1000 through isoreticular expansion of the tetratopic linker (see entries 4-8 in Table 1).[48] To accomplish this criterion, three different approaches were performed to design the extended tetratopic linkers with chelating benzoic acid moieties via (i)

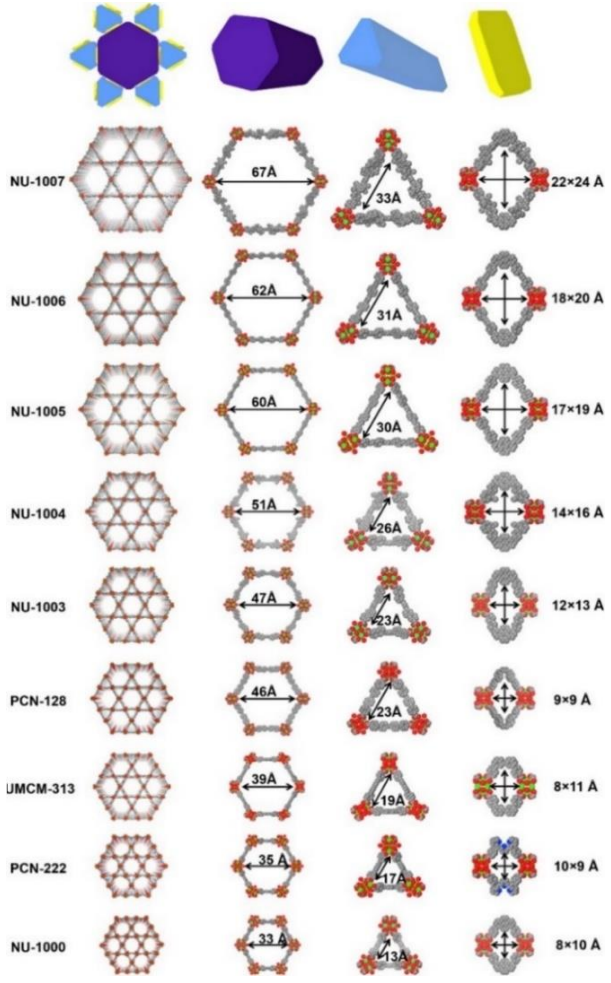

Figure 2. Isoreticular expansion of tetratopic-Zr MOFs of the NU-1000 topology. Reproduced with permission.[48] Copyright 2018, Cell.

aromatic functionalization as shown in L2 and L3 (**Figure 2**); (ii) extended conjugation chemistry, as shown in L4 and L5; (iii) design of the torsion angle, as shown in L6. As displayed in **Figure 2**, NU-1007 has the largest of all hexagonal pore, triangular pore and pore window of 6.7, 3.3 and 2.2 x 2.4 nm, respectively (see entry 8 in Table 1). Remarkably, lactate dehydrogenase (LDH) immobilized in NU-1007 showed the highest rate of coenzyme regeneration, in contrast to that of the LDH@NU-100x (x = 3, 4, 5) as well as the free enzyme. The observed high coenzyme regeneration activity in LDH@NU-1007 is reasoned to be due to the larger pore sizes of NU-1007, which facilitate the molecular traffic of substrate and accessibility to coenzymes (e.g. NAD and NADH), leading to faster kinetic reaction rates.

Zhou and co-workers employed the meso-tetra (4-carboxyphenyl) porphyrin (TCPP) linker to synthesize the mesoporous metalloporphyrin PCN-600 (PCN = porous coordination network) with a large one-dimensional channel of 3.1 nm (see entry 9 in Table 1).[49] PCN-600 with stp topology network is built from six-connected trigonal prismatic nodes and four-connected square planar nodes connecting to four-connected tetrakis (4-carboxyphenyl) porphyrin linkers. It shall be noted that due to its large mesopore, PCN-600 collapses under the normal activation process. PCN-600 can only be activated via supercritical carbon dioxide extraction and treatment with a diluted acid solution. Nonetheless, PCN-600 showed no framework deterioration or phase change at pH 2 and 11, confirming its robustness and chemical stability despite its large pore size. PCN-600 demonstrated high enzyme mimetic activity in the co-oxidation (using H_2O_2 as an oxidant) of phenol and 4-aminoantipyrine substrates towards quinone-imide. The adequate distribution of active sites in the regular mesoporous framework favor the diffusion of the reactants, although with lower diffusion rate of the product with respect to the enzyme Cyt c.

The same group also synthesized another metalloporphyrin-based Zr-MOF with even larger 1D mesoporous channels, with 3.7 nm size in PCN-222 (entry 10 in Table 1).[50] PCN-222 was constructed from 12-connected Zr_6 clusters similar to the building principle of UiO-66. However, in PCN-222, eight edges of the Zr_6 octahedral clusters are coordinated with tetrakis(4-carboxyphenyl)porphyrin (TCPP) linkers, and terminal hydroxy groups as the counter-ions, saturating the rest of the positions. As a result, the symmetry of the Zr_6 carboxylate decreases from Oh to D_{4h}, to accommodate the formation of large mesopores. Astonishingly, PCN-222 showed exceptional water and low pH (pH= 1) stability. The superior chemical stability of PCN-222 could be attributed to the unique coordination chemistry: when viewing the 3D framework along the ab plane, stacked of zirconium-carboxylate layers are observed to form a Kagome-type pattern which is pillared by TCPP ligands. The high chemical stability of PCN-222 was exploited for catalyzing the oxidation of a variety of substrates, such as pyrogallol (3,3,5,5-tetramethylbenzidine) and o-phenylenediamine, outperforming hemin in aqueous media. The high density of active sites, one per 1286 Da, in the case of the mesoporous MOF may be the reason for its higher activity with respect to natural horseradish peroxidase, with only one active site per 44174 Da.

The superior catalytic performance of PCN-222 with respect to benchmark Zr-MOFs is due to (i) its large channels, which greatly facilitate the diffusion of substrates; and (ii) the decorated channels with accessible high density of catalytic acid sites (i.e. hydroxyl groups). By elongating the tetratopic carboxylate porphyrin linker TCPP, and positioning the vicinal phenyl rings and carboxylate groups conformation, the four carboxylate groups present in these extended linkers could be positioned in the same coordinate plane to that of the porphyrin function. This enables the crystallization of another series of isoreticular porphyrinic mesoporous MOFs denoted as PCN-228, PCN-229, and PCN-230 (see entries 11-13 in Table 1).[51] The MOFs exhibit mesopore sizes from 2.5 to 3.8 nm, thanks to the ultra-large linker size. Despite the large mesopore size of PCN-230, it is stable in both acidic and basic medium, indicating extraordinary stability in contrast to other porphyrinic MOFs.

In another work by De Vos and Fischer, the porphyrin-based PCN-222(Rh) MOF, with small trigonal micropores and large hexagonal mesopores, exhibit exceptional diastereoselectivity of dr=42 : 1 (trans : cis) for the cyclopropanation of 4-amino styrene with ethyl diazoacetate.[52] The well-defined channel-like pore geometries including such TCPP-based MOFs (i.e. PCC-222 and PCC-224) favor the substrate driven coordination to Rh catalytic sites in the confined spaces with specific size and geometry. For example, the pore geometry and topology of PCC-22 with large hexagonal mesopores (19 x 32 Å) and small trigonal micropores (9.7 Å) provides Rh-Rh distances that matches the dimensions of the substrates (~10Å). In addition to that, the positioning of functional groups attached to the substrates, controls the diastereoselectivity for this carbene mediated reaction.

Dinca and co-workers synthesized a mesoporous MOF-74 analog from *N*,*N*′-bis(3-carboxy-4-hydroxyphenyl)-1,4,5,8-naphthalenetetradicarboximide linker denoted as NDISA (entry 14 of Table 1).[53] NDISA, with one-dimensional channels having a 3.3 nm pore diameter, is twice the size of MOF-74. The same group also synthesized another mesoporous MOF denoted as MIT-25 (MIT= material of Massachusetts Institute of Technology) from tetrathiafulvalene-tetrabenzoate (TTFTB) linker (entry 15 in Table 1).[54] Twelve carboxylates in each TTFTB triad are connected to four Mg(II) ions, and each octahedral Mg(II) ion is connected facially to two independent TTFTB triads forming a 3,3,6-connected network with ssp topology. Although two **s**sp nets are found interpenetrated, MIT-25 has a mesoporous structure with a pore dimension of 2.64 nm x 3.05 nm, running parallel to the smaller pore apertures of 0.5 nm x 0.56 nm with occluded hydronium counter ions.

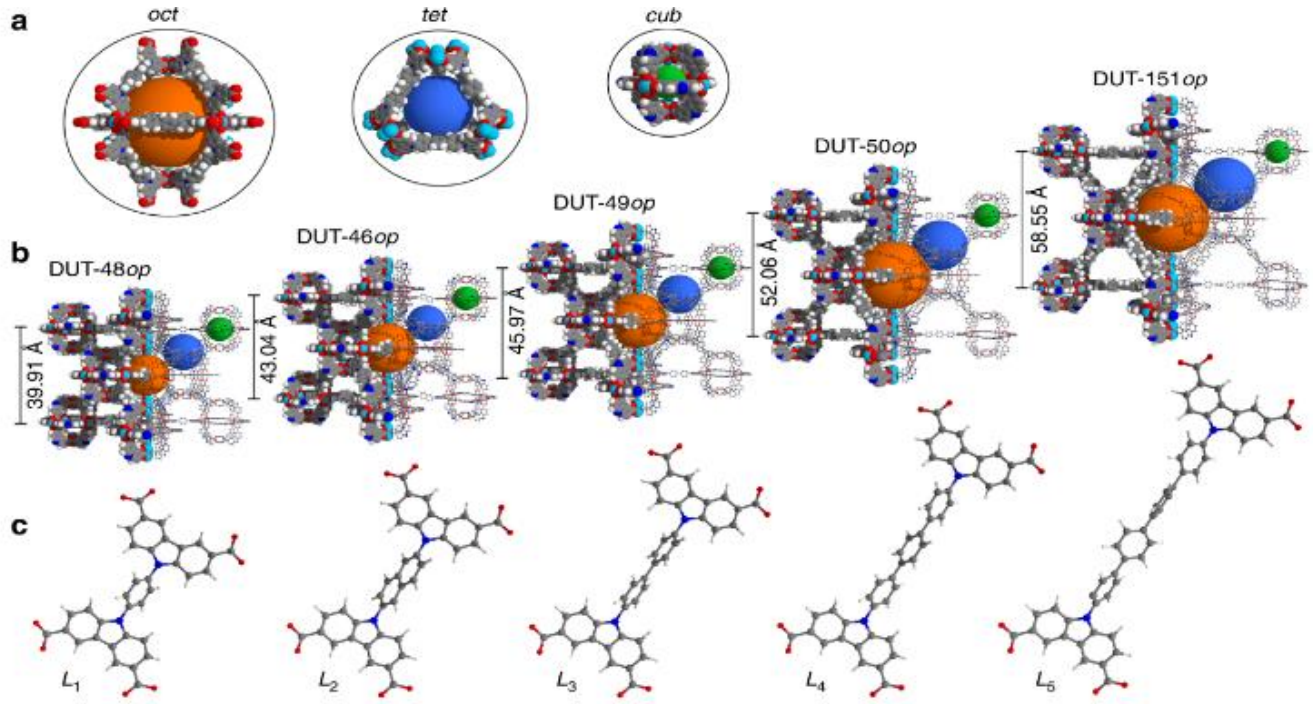

Figure 3. a) Trimodal pore system of isoreticular DUT-49 derivatives: octahedral (oct, orange), tetrahedral (tet, blue), cuboctahedral (cub, green). b) Crystal structures of open pore of DUT-48, -46, -49, -50, and -151 from left to right including respective lattice parameter of the cubic unit cells. c) Conformation of ligands L1–L5. Reproduced with permission.[55] Copyright 2019, Nature.

Through a systematic linker expansion approach, Kaskel and co-workers designed a new isoreticular series of five mesoporous MOFs coined as DUT-46, -48, -49, -50 and -51 MOFs (DUT = Dresden University of Technology) as depicted in **Figure 3.**[55-59] According to the crystal refinement of DUT-48, the authors systematically increased the number of 1,4-substituted phenylene units in the linker of the DUT MOF backbone from one (DUT-48) to four units (DUT-151) as demonstrated Figure 3. These isoreticular MOFs are constructed from bridging the copper paddlewheels to carbazole-3,6-dicarboxylate linker to form metal-organic polyhe-

drons (MOPs) containing small cuboctahedral pores, tetrahedral and octahedral cavities.[55] The pore length of the isoreticular mesoporous MOFs was successfully extended from 3.99 (DUT-48) to 5.85 nm (DUT-151) with increasing linker length. DUT-49 showed high excess of H_2, CO_2 and CH_4 uptake up to 80 mg·g^{-1} (77 K, 50 bar), 2.01 g·g^{-1} (298 K, 50 bar) and 308 mg·g^{-1} (298 K, 110 bar), respectively.[57]

Long and co-workers demonstrated isoreticular synthesis of a mesoporous Zn_2(dobpdc) (dobpdc = 4,4′-dioxidobiphenyl-3,3′-dicarboxylate) MOF having a pore size of 2.2 nm, larger than its structural analog Zn_2(dobdc) (dobdc = 2,5-dioxidobenzene-1,4-dicarboxylate) with a pore diameter of 1.5 nm (entry 20 in Table 1).[60] The diffusivity of CO_2 gas increases by 50 % with increasing the pore diameter from 1.5 nm in Zn_2(dobdc) to 2.2 nm in Zn_2(dobpdc), as observed in the pulsed-field gradient NMR spectra. The enhanced self-diffusion coefficient for CO_2 diffusion in the MOF, with a value of $6\cdot10^{-9}$ m^2·s^{-1} is comparable to the diffusion coefficient of liquid water ($2.3\cdot10^{-9}$ m^2·s^{-1}), showing great potential to overcome mass transport limitations in gas separation and catalysis.

Through topological analysis, Zhou and co-workers discovered another unique approach to design a new zeotype mesoporous MOF by decreasing the symmetry and connectivity of the Zr_6 cluster in order to achieve a compatible zeolite network with tritopic organic linkers. A Zr-based mesoporous MOF denoted as PCN-777 was successfully prepared from a synthesis mixture having high zirconium to 4,4′,4′′-s-triazine-2,4,6-triyl-tribenzoate (TATB) linker ratio (entry 22 in Table 1).[61] The structure of PCN-777 was resolved by a combined synchrotron powder X-ray diffraction and 3D electron diffraction techniques. In particular, PCN-777 is constructed from super-tetrahedra vertexes which consist of four D_{3d} Zr_6 building blocks connected to the TATB linkers along the coordination plane. The final positively charged framework structure is neutralized by two hydroxyl groups. The location of the carboxylates and terminal OH enables the formation of an antiprismatic coordination geometry to assemble super-tetrahedra with the symmetric Zr_6 clusters (D_{3d} form) β-cristobalite topology. PCN-777 possesses a large mesoporous cage (3.8 nm) and a high pore volume (2.82 cm^3 g^{-1}).

Apart from commonly used carboxylate-based linkers employed for mesoporous MOF synthesis, the use of softer ligands such as azolate-type linkers has also been demonstrated to be useful in the design of stable mesoporous MOFs. The coordination chemistry involving azolate-based linkers provides a favorable environment for coordination bond formation with the metal ions, such as Zn^{2+}, due to soft-soft acid-base interactions, resulting in the formation of MOFs with high hydrolytic stability. These unique soft-soft acid-base interactions also allow the generation of new isoreticular MOF series with tunable organic functionalities and pore sizes. This, in principle, could overcome benchmark uptake capacities, molecular diffusions and adsorption selectivity to a guest molecule.[62] For example, -NH_2, -NO_2, -SO_3 and -OH containing ZnBDP azolate-type MOFs have been prepared in the form of straight chains of tetrahedrally coordinated Zn(II) ions in a square-lattice topology (entry 22 in Table 1).[63] The high thermal stability of the isoreticular series (stable up to 420 °C) is attributed to the rigid tetrahedral stereochemistry of the ZnN_4 and the polyconnected nature of the tetragonal lattice. On the one hand, the stability is combined with high flexibility in the case of the amino-functionalized ZnBDP_NH_2, upon solvent removal (changing its structure respect to the solvated one). The amino tagged MOF shows a reversible structural flexibility, while ZnBDP with NO_2- and OH-functional groups exhibit a reversible volume shrinkage. The catalytic properties of the mesoporous NiBDP containing open metal sites, as well as confined species were explored in the nitroaldol condensation and hydroamination of alkynes, resulting in higher turnover numbers with respect to microporous MOFs or zeolites.[64, 65]

Other azolate MOFs such as Cu(BTDD)$_2$, known as MIT-20, has the same topology as the MOF-74 series.[66] In this structure, Each Cu^{2+} adopts a distorted square pyramidal geometry with two chloride atoms occupying the axial positions, and the quadrilateral base is formed by three nitrogen atoms from three independent ligands and one oxygen atom (entry 23 in Table 1). The resulting Cu SBUs are linked by $BTDD^{2-}$ linkers, forming one-dimensional hexagonal channels with a diameter of ca. 2.2 nm and anionic framework balanced by free dimethylammonium cations or other cationic host species.

2.3. Mixed-linker approach

Integrating two (or more) different linkers to single metal ions/clusters is an efficient approach to synthesize multifunctional MOFs with tailorable topology, tunable pore size and functionality. The occurrence of defects and disorder accompanied with the mixed-linker approach, where the linker of a well-known framework is partially substituted by a linker having a different coordinating group, is an exciting concept for tailoring material properties for adsorption and catalysis, among other physico-chemical properties.[67-69] The selection of linkers with distinct length and ratio is crucial to ensure cooperative linking chemistry to the metal nodes and afford the design of a new mesoporous MOF. However, in most cases the synthesis involving the use of two different linkers would often yield: (i) single-phase multivariate microporous MOFs, (ii) heterogeneous MOF crystals of different crystalline phases due to competitive crystallization and (iii) interpenetrated frameworks. This mixed-linker approach was first introduced by Matzger and co-workers to synthesize mesoporous MOFs with large cavities within a single phase pure crystal denoted as UMCM-1 and UMCM-2 (UMCM= University of Michigan Crystalline Material).[70, 71] For example, the UMCM-1 was synthesized from terephthalic acid (BDC) and 1,3,5-tris(4-carboxyphenyl)benzene (BTB) linkers in the presence of Zn (entry 24 in Table 1). It shall be noted that, BDC and BTB linkers are used to synthesize bulk microporous MOF-5 and MOF-177, respectively in the presence of Zn(II). UMCM-1 is constructed from the octahedral arrangement of bridged Zn_4O clusters to two BDC and four BTB linkers. Assembly of six octahedra results in the formation of one-dimensional hexagonal mesopores with an internal pore dimension of 2.7 nm x 3.2 nm in addition to the micropores (1.4 nm x 1.7 nm) located in the cage-like structures of the octahedral.[70] Phase-pure UMCM-1 material is only formed when the synthesis mixture contains a mole ratio 1 < BDC:BTB < 1.5. UMCM-2 was synthesized by substituting

the ditopic linker BDC linker with thieno[3,2-b]thiophene-2,5-dicarboxylate (T^2DC) at a mole ratio of T^2DC:BTB equal to 1 (entry 25 in Table 1).[71] UMCM-1 has been reported as an active and stable catalyst for the cycloaddition reaction of CO_2 with propylene oxide at room temperature using tetrabutylammonium bromide as a co-catalyst to afford 85% yield of propylene carbonate after 24 h.[72] The superior catalytic activity and selectivity of UMCM-1 in comparison to the other MOFs, e.g. MOF-5 and IRMOF-3, is attributed to the presence of the secondary mesopores. The mesopore channels of UMCM-1 facilitate molecular diffusion while the catalytic reaction occurs predominantly in the intrinsic micropores of UMCM-1. However, it shall be noted that the open metal sites (Lewis acid sites) predominantly located in the micropores are responsible for the activation and ring opening of the epoxides while the covalently bound amine functional groups (Brønsted acid sites) of organic linkers present in the micropore structure facilitate the interaction and polarisation in the step of CO_2 fixation. The synthesis of UMCM-1 with cooperative amino functions, denoted as UMCM-NH_2, has been reported by Cohen and co-workers via substituting BDC linker with NH_2-BDC.[73, 74] This derivative UMCM-1-NH_2 MOF can be successfully modified by introducing 3-hydroxyphthalic anhydride and 2,3-pyrazinedicarboxylic anhydride, to give novel MOFs named as UMCM-1-AMsal and UMCM-1-AMpz via a post-synthetic modification approach. As described by the same group, the functional mesoMOFs catalyze the Mukaiyama-aldol reactions with mesitaldehyde or 1-naphthaldehyde and 1-methoxy-2-methyl-1-(tri-methylsiloxy)propene at room temperature. This work has been discussed in detail in the review paper published by the same group.[75]

Kaskel and co-workers developed similar concepts for the synthesis of mesoporous MOFs named DUT-6 and -32.[76, 77] DUT-6 is formed from Zn_4O^{6+} clusters coordinated to 2,6-naphthalenedicarboxylate (NDC) and BTB linkers, resulting in large dodecahedral mesoporous cages of 2.5-3 nm in diameter interconnected via smaller micropores (entry 26 in Table 1).[76] DUT-32 was synthesized from 4,4′-biphenylenedicarboxylic acid (BPDC) with another tritopic 4,4′,4″-[benzene-1,3,5-triyltris(carbonylimino)]tris-benzoate) linker in the presence of zinc nitrate.[77] Interestingly, the structure of DUT-32 consists of two symmetry-independent Zn_4O arranged in both *trans* and *cis* orientations at the cluster position relative to each other, forming a 3D framework with three different mesopore sizes (3 nm x 4 nm, 2.8 nm x 3.2 nm and 2 nm x 2.6 nm) and one smaller micropore of 1.4 nm x 1.8 nm (entry 27 in Table1). In terms of adsorption, DUT-6 and -32 showed a similar maximum excess methane capacity of 0.24 $g \cdot g^{-1}$ at 25 °C and 100 bar.

Through the isoreticular expansion of the tritopic BTB linker to 4,4′,4″-[benzene-1,3,5-triyl-tris(ethyne-2,1-diyl)]tribenzoate (BTE) and mixing with BPDC linker in a reaction with zinc nitrate, the mesoporous MOF-210 was first reported by Yaghi and co-workers.[78] The pore dimension obtained in the final material was of 2.69 nm x 4.83 nm, which is the largest mesocage ever reported among other mesoporous MOFs synthesized via this mixed-linker approach (entry 28 in Table1). The surface excess hydrogen and methane uptake in MOF-210 at 80 bar were 86 $mg \cdot g^{-1}$ at -196 °C and 264 $mg \cdot g^{-1}$ at 25 °C, respectively. Recently, Kaskel and co-workers synthesized a mesoporous MOF named as DUT-60 with the highest recorded BET area and pore volume of 7839 $cm^2 \cdot g^{-1}$ and 5.02 $cm^3 \cdot g^{-1}$, respectively, surpassing all known crystalline framework materials (see entry 29 of Table 1).[79] DUT-60 was synthesized from an expanded tritopic 1,3,5-tris(4′-carboxy[1,1′-biphenyl]-4-yl)benzene (BBC) linker and a ditopic 1,4-bis-*p*-carboxyphenylbuta-1,3-diene (BCPBD) linker in the reaction with zinc nitrate. DUT-60 is a truly mesoporous MOF, containing large mesopores with a pore dimension of 3.7 nm x 4.2 nm interconnected with smaller mesopores having a pore dimension of 1.5 nm × 2.7 nm. The successfully designed stable mesoporous MOFs based on this concept is mainly restricted by the implication of topologically distinct di-and tritopic linkers with identical coordination chemistry to Zn_4O clusters at specific linker ratio range.

To conclude this section, we will discuss the use of the mixed-linker approach to improve the porosity and catalytic activity of the bulk MOF or surface-mounted MOF thin films.[80] The introduction of defect-generating linkers such as pyridine-3,5-dicarboxylic acid in $Ru_3(BTC)_2$ do not compromise the overall integrity and robustness of the framework.[81, 82] However, small loops occur between adsorption and desorption isotherms of the defective MOF, together with an increase of the total pore volume (from 0.3 to 0.5 $cm^3 \cdot g^{-1}$) and an average pore diameter (from 1.8 to 2.3 nm), right into the mesopore regime. The lowered coordination number of Ru active sites in the defective MOFs improves its catalytic performance towards the conversion of olefins and carbonyls.[83, 84]

2.4 Modulator-induced defect engineering (MIDE)

Modulated synthesis approach has become a hot research topic in the recent years to fine-tune the pore properties of MOFs, which incorporate defects of various types and length scales (in line with the strategy named as "defect-engineering) for adsorption and catalysis, among other chemical properties.[67-69] The MIDE approach is also referred to as "fragmented linker co-assembly method" where the linker of the parent framework is partially substituted by another defective linker having a different coordinating group to create defects and disorder in the MOF crystals. The defective MOFs exhibit open metal sites and hierarchical micro/mesopore structures correlated with the nature and the degree of defective linker incorporation into the framework.[85] One approach of this strategy is mainly based on the addition of monocarboxylic acids as crystal growth modulators into the synthesis mixture or defective linkers such as isophthalate, 3,5-pyridinedicarboxylic acid or 5-hydroxyisophthalic acid. During the MOF synthesis, these modulators are incorporated into the framework via competitive coordination with the linkers (either ditopic, tritopic or tetratopic) to the bridging metal nodes/clusters and ultimately to create defects in the crystal structure or surface-mounted thin films.

The MIDE approach leads to a final MOF framework in which the polycarboxylate linkers are partially replaced by the modulator, usually a monocarboxylate molecule such as formic, acetic, trifluoroacetic or benzoic acid.[86-92] For example, Van de Voorde *et al.* have demonstrated that the incorporation of the modulator (e.g. trifluoroacetic acid) in the

zirconium dicarboxylate MOFs (e.g. UiO-66) can substantially enhance the mechanical stability of the frameworks as the introduced acid-based modulators can strengthen the Zr–O bonds between Zr(IV) clusters and carboxylates in UiO-66 via a local electron-withdrawing effect.[89] Both the incorporation and/or the subsequent removal of modulators can generate defects within the framework, resulting in a MOF material with mesopores that potentially improve its performance in gas adsorption and catalysis.

Jiang and co-workers demonstrated the preparation of hierarchical UiO-66 by adding long-chain fatty acids (e.g. octanoic acid, dodecanoic acid or palmitic acid) into the synthesis mixture containing $ZrCl_4$ and BDC.[93] Residual fatty acids trapped inside UiO-66 were subsequently removed by treating the obtained powder in a solution containing concentrated HCl in DMF and heated at 90 °C for 12 h. The role of the BDC linker amount was studied for a given Zr/dodecanoic acid mole ratio of 1:35 while manipulating the mole ratio of Zr/BDC was screened from 1:1, 1:0.8, 1:0.5 to 1:0.3 to investigate the optimal synthetic conditions for the preparation of hierarchical UiO-66 with large mesopores. The authors discovered an optimal Zr/BDC ratio of 1:0.5, based on the clear hysteresis loop present at the measured N_2 sorption isotherms, indicative of mesoporosity, and DFT pore size distribution showed an average pore size of 5.5 nm in width. The impact of the fatty acid chain length on the mesopore generation was studied by varying the fatty acid moieties, while the molar ratio of Zr/BDC ratio was kept at 1:0.5.

N_2 sorption isotherms and pore size distributions of the UiO-66 synthesized in the presence of octanoic acid, dodecanoic acid or palmitic acid (with large alkyl chains of 8-12 carbon atoms) generates the hierarchical UiO-66 with the largest mesopore (5.5 nm) when the alkyl chain length gradually increases from 8 to 12 carbon atoms. The pore filling effect of the alkyl chain of the modulator led to a large mesopore generation, through $Zr_6O_4(OH)_4$ and BDC disconnections, after the extraction of the long alkyl chain carboxylic acid modulator. Nevertheless, upon adding the palmitic acid (with even longer fatty acid chain of 16 carbon atoms) as a modulator, no increase of mesoporosity was observed, since the mesopore diameter decreases from 5.5 to 4 nm. The reason for that was provided by the authors, which considered a key factor in the low acid solubility and weaker interaction of palmitic acid with the $Zr_6O_4(OH)_4$ clusters. Interestingly, when a monocarboxylic acid (i.e. acetic acid) was added into the synthesis mixture, no mesoporosity was noted as confirmed by N_2 sorption isotherm.

The hierarchical UiO-66 was used as a host to encapsulated HPW via the impregnation method and showed an improved catalytic performance for the alcoholysis of styrene oxide, outperforming the microporous HPW@UiO-66. Moreover, the catalytic performance of hierarchical UiO-66 *vs.* classic microporous UiO-66 was studied in reactions between 1,3-cyclohexanedione and short or large α,*β*-unsaturated aldehydes (e.g. 3-methyl-2-butenal or cinnamaldehyde). Although UiO-66 and hierarchical UiO-66 showed similar catalytic activity for small substrates (i.e. 3-methyl-2-butenal), hierarchical UiO-66 achieved a higher conversion (70%) when a larger substrate was used (i.e. cinnamaldehyde) with respect to UiO-66 (20%), indicating the key role played by the hierarchical pores to decrease the energy during the molecular traffic of bulky substrates/products.

Zhou and co-workers reported the preparation of hierarchical PCN-125 via the addition of smaller size linker fragments (R-isophtalic acid, R being the functional groups such as aminomethyl, nitro, sulfo, and sodium sulfo groups) into the synthesis mixture containing the primitive ligand terphenyltetracarboxylic acid (TPTC) and copper nitrate hexahydrate (entry 30 in Table 1).[94] For example, nitro functionalized PCN-125 possessing large mesopores with 20 nm in diameter in addition to its intrinsic micropores of 1 nm was synthesized by varying the TPTC and nitro-isophthalic linker fragment ratio from 5.5 to 19.5. On the other hand, PCN-125 with a smaller mesopore size of 5.8 nm was obtained when aminomethyl-isophtalic acid linker fragment was utilized. All R-isoph-PCN-125 showed an improved CO_2 uptake and heats of CO_2 adsorption at 273 K and 130 mmHg in comparison to unfunctionalized PCN-125. For example, amino-PCN-125 adsorbed 30% more CO_2 at 130 mmHg than the unfunctionalized PCN-125 (26 $cm^3 \cdot g^{-1}$) while nitro-PCN-125 recorded the highest heat of CO_2 adsorption (32.5 kJ/mol), which was 50% higher than the unfunctionalized PCN-125. For the interest of defective MOFs, readers can refer to review papers by Fischer and co-workers which discuss in detail on the synthesis and characterization of defective MOFs as well as their role play in improving their catalytic and adsorptive performance in comparison to their parent materials.

2.5 1D-2D-3D topotactic transformations

Solid-solid structural transformations in MOFs, e.g. 1D-2D, 1D-3D, 2D-2D, 3D-3D, 3D-amorphous, 3D-amorphous-3D, remains a hot topic in solid-state chemistry as it allows for direct visualization of how the crystal structure changes when subjected to external stimuli (e.g. heat, light, pressure) and guest uptake/removal.[95-98] In general, MOF-transformations involve significant rearrangements of molecular building blocks in the crystals, which include structural rotation, bending, swinging, sliding, shrinking, or swelling. However, one of the utmost criteria to achieve successful crystal transformations is to withstand the stress during phase transition to maintain its crystalline structure throughout the transformation process. Otherwise, the initial crystal loses its crystallinity and become amorphous, e.g. transformation of ZIF-8 (zeolitic-imidazolate framework-8) to amorphous ZIF-8.[99-101]

Recently, Wee et al. reported a thermoinduced 1D-2D-3D transformation for the synthesis of a new hierarchical copper benzentricarboxylate MOF coined as COK-18 (COK-18= Centrum voor Oppervlaktechemie en Katalyse No. 18).[102] COK-18 was synthesized via thermoinduced solid–solid transformation of a non-porous crystalline CuBTC precursor known as H1 phase. The H1 precursor material was prepared from room-temperature crystallization of copper nitrate and BTC linker dissolved in a water/ethanol solution. A thermal treatment (at 120 °C for 48 h) of this precursor solution resulted in the formation of COK-18 with a synthesis yield above 95% based on Cu. According to Rietveld refinement of the powder XRD pattern, COK-18 crystallizes in the orthorhombic space group *Immm* instead of the cubic space group $Fm\bar{3}m$ found in the microporous HKUST-1. Each of the copper paddlewheel in COK-18 is connected to

two BTC linkers instead of the four found in the conventional microporous HKUST-1. The positively charged framework is counterbalanced by the hydroxyl groups, resulting in a microporous structure with a rhombus pore shape.

The nitrogen adsorption–desorption analysis of COK-18 showed a Type I isotherm, which is the typical characteristic of a microporous material. An additional hysteresis loop was observed originating from the mesoporosity present in the MOF. COK-18 has a micropore size of 1.1 nm, next to the large mesopores of 12 nm wide (entry 31 in Table 1). The observed type H4 hysteresis further indicates that the largest mesopores have a slit-like pore shape interconnected through smaller micropores, as confirmed by electron tomography. A combination of X-ray crystallography, N_2 physisorption analysis and SEM provides a detailed insight into the underlying thermoinduced phase transformation mechanism. SEM imaging revealed significant morphological changes of the solids recovered from different solvothermal synthesis times (3, 6, 9, and 12 h).

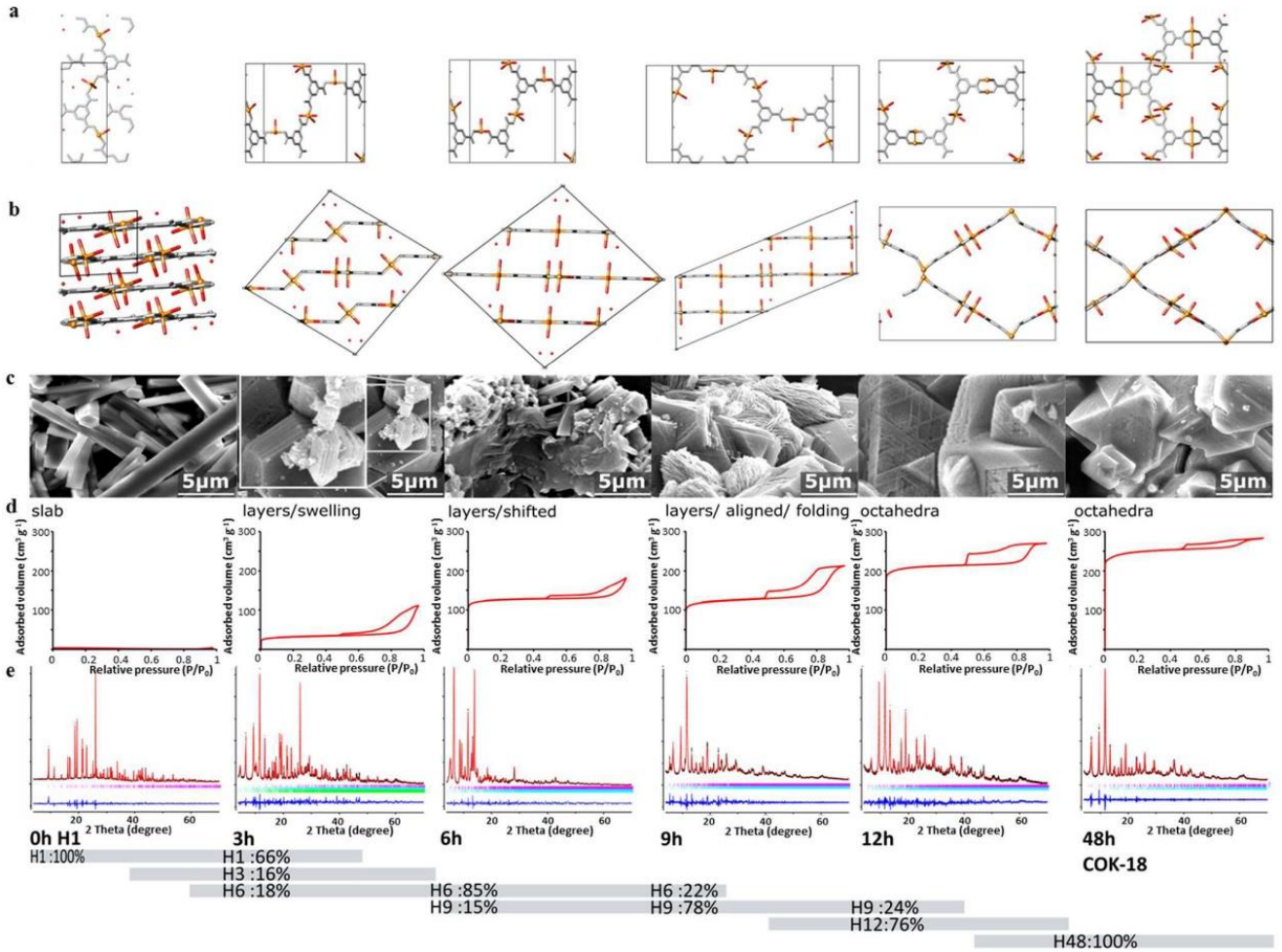

Figure 4. Crystal structures with (a) top and (b) side views of the Cu-BTC ribbons. (c) SEM images, (d) nitrogen physisorption isotherms, (d) Rietveld refinements, and phase composition at different synthesis times of 0, 3, 6, 9, 12, and 48 h (from left to right). Reproduced with permission.[102] Copyright 2017, ACS.

For instance, the dense precursor phase (which appears as lamellae), was swelled after 3 h to resemble stacked of hexagonal layers, contributing to a significant enhancement in micro and mesoporosities (**Figure 4**). After 6 h, these stacked of hexagonal layers were sheered into undulating hexagonal sheets. These hexagonal sheets were realigned into the flake-like structure but without expressed facets after 9 h. After 12 h, spongy octahedra with a substantial increase in micro- and mesoporosities were formed. All the recovered solids at different synthesis times were highly crystalline, according to the measured XRD patterns. Rietveld refinement confirmed that the planar zigzag ribbons-BTC linkages found in the H1 phase were preserved throughout the transformation process. The arrangement of copper and BTC within 1D ribbons, forming the coordinatively bound hexagonal layers, was elucidated by Rietveld refinement as the main molecular building blocks found in COK-18. Rietveld refinements proved a transformation scheme consisting of the folding of the nanoribbons (with *b*-axis around 0.19 nm) into COK-18 octahedra, which are consistent with the experimental results.

The separation properties of COK-18 in comparison to microporous HKUST-1 adsorbent were tested by using a complex gas mixture containing 11 C_1–C_6 alkanes. The wide channels accessible through smaller micropores, in combination with the induced chemical functionality (e.g. unsaturated Cu(II) sites and hydroxyl functions decorated on the pore walls) of the COK-18 structure, contributed to improved mass transport of the evaluated alkanes. A relatively low adsorption enthalpy and entropy necessary for a multicomponent hydrocarbon mixture separation process at low temperatures were achieved. For example, the adsorption

enthalpy of the C_6 alkanes on COK-18 was below 51 kJ·mol^{-1} (e.g. *n*-hexane, ΔH = -50.3 kJ·mol^{-1}). Similar enthalpies were obtained for the comparatively ordered mesoporous silica (e.g. MCM-48) and a hierarchically ordered pure silica material (e.g. Zeotile-2).

On the other hand, HKUST-1 with much narrower micropores showed poor kinetic diffusion especially for the dibranched hexanes and the straight chain hexane, as hinted from the substantial chromatographic peak under similar separation conditions. COK-18 also showed an improved separation of hexane isomers with respect to HKUST-1 adsorbent. Molecular simulations further confirmed that the molecular shape selectivity towards alkane separation was achieved via polarization and configurational entropy effects. The results highlight the importance of an interconnected hierarchical pore system that, on the one hand maximize entropy differences, and on the other hand, enables the optimal molecular transport for the selective separation of a complex hydrocarbon gas mixture.

3. Synthesis of hierarchical MOFs assisted by soft templates

3.1 Alkyl amines as ionic surfactants

Surfactant molecules have been proposed as templates for the controlled generation of mesoporosity in the microporous structure of metal-organic frameworks.[103-105] On the one hand, cationic surfactants (i.e. quaternary amines with long alkyl chains) were first reported almost one decade ago for the synthesis of the copper benzene-tricarboxylate MOF known as HKUST-1 [$Cu_3(BTC)_2$]. Upon addition of the cationic CTAB (cetyltrimethyl ammonium bromide) surfactant into the synthesis solution containing copper(II) nitrate salt and BTC linker subjected to solvothermal synthesis at 120 °C (**Figure 5a**), HKUST-1 with tunable mesopores with diameters ranging from 3.8 to 31.0 nm were synthesized, depending on the CTAB/Cu^{2+} molar ratio.[106]

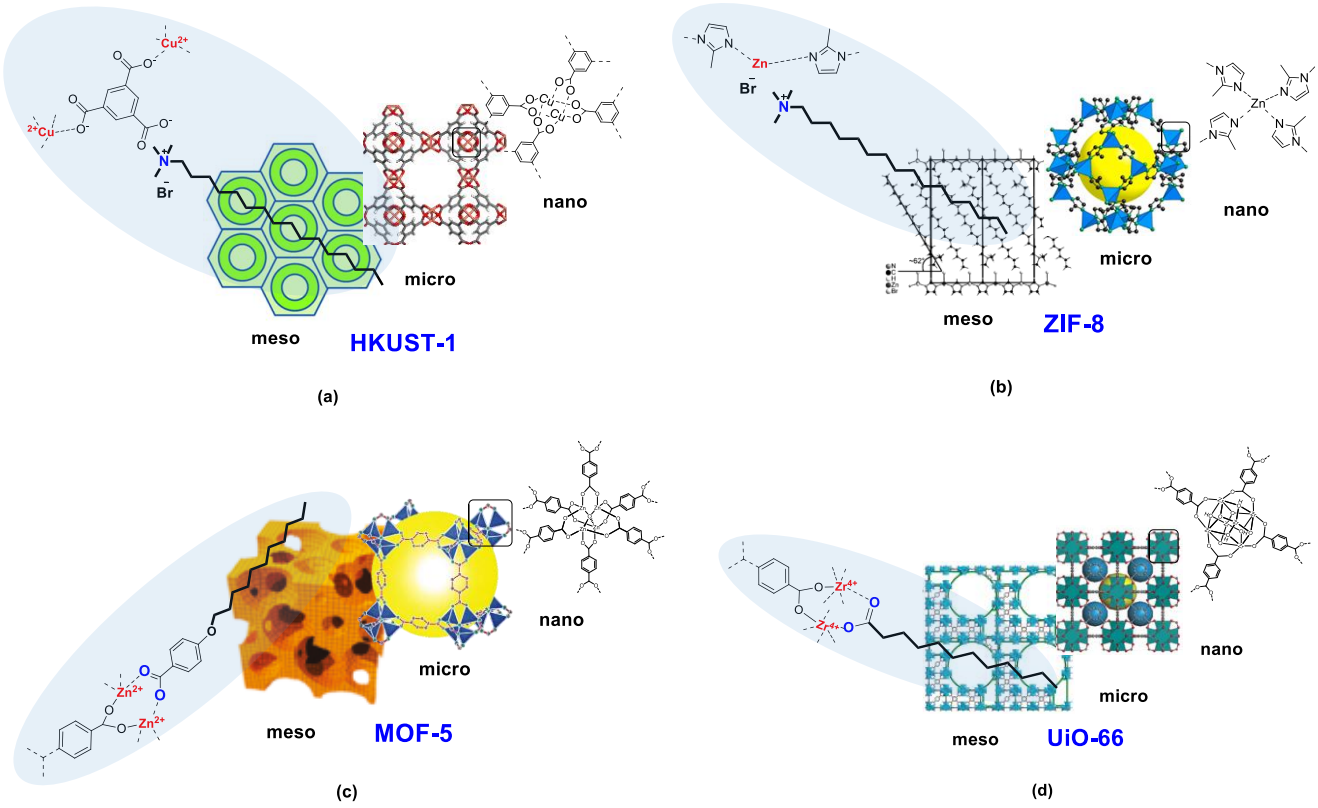

Figure 5. Schematic representation of surfactant-assisted synthesis of mesoporous MOFs. The three levels of hierarchical porosity (nano, micro and meso) generated with the use of long chain amines (a), (b) or carboxylic acids (c), (d) are shown for HKUST-1 (a), ZIF-8 (b), MOF-5 (c) and UiO-66 (d) metal-organic frameworks. Blue shaded areas indicates tentative surfactant-SBUs interactions.

The structure-directing effect of CTAB is attributed to the well-defined chemical interactions between the cationic $C_{18}H_{34}N(CH_3)_3^+$ surfactant and the negatively charged benzenetricarboxylate (btc^{3-}) linker ions. The micelles of the cationic surfactant electrostatically interact with the negatively charged btc^{3-} ions resulting in the spontaneous formation of microporous MOF nanoparticles. The self-assembly of the disordered mesostructures in the continuous interphase between micelles and framework-building blocks (e.g. Cu^{2+} metal ions, btc^{3-} organic ligand) induces the formation of the hierarchical $Cu_3(btc)_2$ structures.

On the other hand, Wee et al. reported a dual templating approach using Keggin ions in addition to the CTAB surfactant for the structural motif of the HKUST-1.[107] The authors employed Keggin ions as molecular templates in order to define the structural motif of the final mesoporous MOF. This is due to the exact Kegging ion fitting into one of the cage-like pores, in the presence of CTAB to direct these units into an ordered mesoporous structure achieved via "void filling" mechanism. The favored interaction between the CTA^+ and the $[Cu_{46}(C_9H_3O_6)_{24}(OH)_{12}]$ $(PW_{12}O_{40})_3^-$ units is attributed to

the charge balancing between them. Interestingly, the resultant ordered mesoporous structure COK-15 achieved superior catalytic performance for the quantitative conversion of styrene oxide (100 % conversion). This is due to the catalytic activity of the coordinatively unsaturated copper paddle wheels and hydroxyl groups positioned on the mesoporous walls. In contrast, the microporous HKUST-1 HPW@$Cu_3(BTC)_2$ only converted 40% of the substrate, under similar reaction conditions. In the case of the microporous HKUST-1, the resulting conversion was < 2% conversion.

An interesting case of hierarchical design is that of mesoporous ZIFs, which possess a more robust zeolite-like structure formed by soft-soft Zn-N acid-base interactions. Mesostructured imidazolate frameworks (MIFs) are formed from zinc imidazolate chains or layers in between CTAB, constituting a mesoscopic layered hybrid MCM-like lamellar silica mesophase.[108] The generation of non-conventional zinc imidazolate chains, i.e. $Zn(C_4N_2)_{2/2}$, instead of classic zinc imidazolate motifs, i.e. $Zn(C_4N_2)_{4/2}$, was assumed based on the tetrahedral zinc coordination environment and electroneutrality arguments. The authors assumed that the anionic corner-sharing $[Zn(C_4N_2)_{2/2}Br_2]^-$ chains linked to positively charged CTA^+ ions are the main structural features for the formation of disordered mesostructures. It is worth mentioning that the disordered mesostructure formed next to the microporous crystalline ZIF-8 walls is driven by the electrostatically cooperative assembly process in the presence of CTAB, highlighting the crucial role of this well-reported surfactant. NMR characterization of the MIFs confirmed that the CTA^+ surfactants are in the close proximity to the methylimidazole framework moieties, highlighting the crucial effect of the intimacy between the halogenide counter-ions and the surfactants for optimum interactions.[109]

The CTAB has also been employed in the formation of stable colloidal suspensions containing monodispersed truncated rhombic dodecahedral (TRD) ZIF-8 particles, that eventually self-assembled into 3D superstructures with high crystal packing density. On the contrary, CTAB-free ZIF-8 particle synthesis system failed to achieve packing with a well-defined ordered structure, due to the presence of van der Waals interactions between the ZIF-8 particles, which destabilize the colloidal suspensions.[110]

Mesoporous HKUST-1 framework formation has been possible by contacting a guanidine type surfactant with the carboxylate groups of the BTC linkers, followed by the addition of the Cu^{2+} ion precursor into the synthesis mixture.[111] The authors reported that the presence of surfactant disrupted the framework connectivity during crystal growth as a result of pore-filling effect generated by the selective interaction between the guanidine alkyl chains (of the bulky surfactant). This give rise to structural defects due to a space-filling effect similar to that described for the use of fatty acid modulators of meso-UiO-type MOFs (see section 2.4). Such surfactant-induced defects are responsible for the hollow structure formation upon surfactant removal. The authors suggest that the probable interaction of the surface defects with the water molecules present in the synthesis, would eventually lead to further pore enlargement and generation of meso- and macroscale patterns in the MOF crystals as a result of linker dislocation. The guanidine-HKUST-1 phases presented both Type I and IV isotherms, which indicate the co-existence of the well-known micropores in additional to newly generated meso- and macroscale features (exhibiting pore diameters in the final material between 53 and 73 nm). In contrast, the absence of guanidine-type surfactant results in the classic type-I isotherm obtained for the microporous parent HKUST-1.

We will conclude this section commenting two recent ionic-surfactant templated synthesis of mesoporous MOFs. On the one hand, a novel method to generate mesoporosity employs the ionic liquid 1-octyl-3-methylimidazolium tetrafluoroborate as an electrolyte and as a template via self-aggregation to create mesopores in the electrosynthesis of MFM-100 tetracarboxylate copper MOF.[112] Mesopores of 4.7 nm confirmed the template effect of the ionic liquid, which aggregates match the mesopore size. The hierarchical porosity and the presence of defect sites contribute to the catalytic activity in the oxidation of a broad range of alcohols. On the other hand, another recent work employs the Hofmeister salting-in ion of ClO_4^- and Pluronic poly(ethylene oxide)-poly(propylene oxide)-poly-(ethylene oxide) copolymers as template of mesoporous Ce-UiO-66-type MOFs.[113] This hierarchical MOFs exhibit microporosity and large cylindrical mesopores of 10 nm size, which resulted very efficient in the encapsulation of trypsine for the biodegradation of proteins of increasing size, such as cytochrome c (2.6 x 3.2 x 3.3 nm^3), myoglobin (4.5 x 3.5 x 2.5 nm^3), and bovine serum albumin (5.0 x 7.0 x 7.0 nm^3). This represents a breakthrough in the extension of the concepts of structure directing copolymers in zeolites and mesoporous silica based materials or even MOF/MOF-derived silica based catalysts,[114-116] into the synthesis of bulk mesoporous MOFs with hierarchical porous architectures.

3.2 Fatty acids as surfactants

As a borderline case between ionic and non-ionic surfactants, we will discuss the chemical interaction occurring between the fatty acid surfactants and the MOF precursors in order to generate a mesoporous structure in the case of zinc and zirconium terephthalates (MOF-5 and UiO-66). A well-defined methodology to generate mesoporosity in MOFs has been based on this concept, i.e. the use of long alkyl chain carboxylic acids. In 2011, Yaghi's group first reported the straightforward synthesis of a mesoporous metal-organic framework, with the topology of classic MOF-5 $[Zn_4O(O_2CC_6H_4CO_2)_3]$, from zinc nitrate and terephthalic acid in the presence of aromatic carboxylic acids with large alkyl chains, such as 4-(dodecyloxy)benzoic acid (DBA) as surfactant.[117] The large alkyl chain benzoate $[CH_3(CH_2)_{11}OC_6H_4CO_2^-]$ can directly coordinate by electrostatic interactions to the MOF building blocks $(Zn_4O)^{6+}$ of opposite charge, as shown in the **Figure 5c**. The carboxylic function binds to the zinc ions while the alkyl chain fills the space in the crystalline structure containing meso- and macropores with pore sizes range from 10 nm to 100 nm within the MOF crystals. The mesoporous MOF-5 was deeply characterized by electronic microscopy and CO_2 adsorption, presenting a higher CO_2 uptake capacity than standard microporous MOF-5 due to the filling of the meso- and macro- pores at high N_2 pressure.

Recently, a hierarchical MOF-5 was prepared in the presence of lauric acid ($C_{11}H_{23}CO_2H$) and polyvinyl pyrrolidone (PVP).[118] In this case, the PVP directs the generation of 2D nanosheets while the competitive coordination of deprotonated lauric acid and terephtalic acid to the Zn_4O clusters enable the creation of mesopores. Such mesostructure is created by the favored coordination of terephthalic acid with respect to lauric acid (the weakly coordinated lauric acid dissociates from the cluster) as the synthesis of the MOF proceeds. Although, initially both lauric and terephthalic carboxylates are coordinated to the zirconium oxoclusters, the migration of lauric acid facilitates subsequent acid-promoted etching of the molecular building blocks, enabling the mesopore formation in the nanosheets. This hierarchical MOF was successfully employed as a host for palladium nanoparticles with high activity in the hydrogenation of nitro groups at 1 bar of H_2 and 60 ºC due to the better dispersion of the nanoparticles and reduced agglomeration in the mesoporous matrix.

The use of monocarboxylate containing compounds for the generation of mesoporous frameworks based on zirconium-terephtalate defective networks deserves attention (see section 2.4). Structural defects associated with linkers missing from the nodes and therefore unoccupied coordination sites at metal clusters of Zr MOFs have been detected and intentionally generated to tune the porosity of the final material.[119, 120] Those defects occur as some of the twelve benzenedicarboxylate $(BDC)^{2-}$ linkers that hold together the octahedral $[Zr_6O_4(OH)_4]^{12+}$ inorganic building block are missing from the framework during the synthesis of the UiO-66 Zr MOF. Moreover, when the Zr node is missing one linker, the remaining coordination sites on each node appears to be occupied by the monocarboxylate (i.e. acetic acid) employed in the synthesis or water molecules directly coordinated to a Zr atom.[121-123] The extraordinary thermal and chemical robustness of the zirconium terephthalate UiO-66 and the versatility of this monocarboxylate-induced defect-formation strategy has been recently used for the tailorable generation of highly stable hierarchical porosity in Zr MOFs.[93]

The reaction between an excess of metal precursors and sub-stoichiometric quantities of organic linkers, in the presence of long alkyl chain monocarboxylic acid as surfactant templates promotes the supramolecular coordination of the carboxylate group ($R\text{-}CO_2^-$) to the Zr oxoclusters $[Zr_6O_4(OH)_4]^{12+}$, while the alkyl chain (R) induces structural defects. This eventually results in the generation of additional pore space next to the micropores (**Figure 5d**). In fact, the coordination bond between a carboxylate group of the surfactant and the zirconium ion in the MOF precursors is favored due to hard-hard Zr-O acid-base interactions, which sterically competes with the pore space of smaller BDC linker (see section 2.4). A pore size up to 8.6 nm is obtained with lauric acid as modulator, which is in line with the very large hysteresis loop in the N_2 sorption isotherm (entry 35 in Table 1). When the alkyl chain length of the carboxylic acid is very short, such as in the case of acetic acid, the mesopore is practically negligible and no indication of hysteresis is observed in the N_2 sorption curves. However, upon adding the very long palmitic acid as a surfactant, the pore diameter further decreases, possibly due to the acid low solubility, as well as poor coordination with the Zr(IV) metal ions. The mesoporous UiO-66 material was able to successfully uptake an iron-containing porphyrine in contrast to the parent UiO-66, which does not promote the oxidation of 3,5,3',5'-tetramethylbenzidine. In addition, the mesoporous MOF containing heteropolyacids as active sites catalyzes the ring opening of styrene with methanol with a better performance than the microporous one.

3.3 Surfactant-free emulsion templates

Novel ZIF-8-based capsular metal-organic structures having void spaces in their interior have been synthesized by treating their molecular building blocks in an oil-in-water emulsion medium, without needing pre-formed MOF particles.[124] This strategy allows systematic control of the N-H hydrogen bond donation (or proton exchange) from the imidazole linker to the water medium, which determines the ease of coordination with Zn^{2+} Lewis acid cations. As a result, the Zn-imidazole framework generated was etched in the water medium at random domains within the crystals. This phenomenon occurs especially at the boundaries between particles, resulting in a MOF with a controlled capsule size and shell thickness. The framework stability and purity of the resulting hollow capsules revealed a phase-pure ZIF-8 with the sodalite topology, as confirmed by XRD. The formation of well-defined hollow capsular structures with mean values between 0.75 and 1.25 μm in diameter and with a shell thickness of approximately 100 nm, was observed with the help of SEM imaging.

3.4 Hydrogels

The use of hydrogels as templates, known as template emulsification method, for the creation of hierarchical Zn-MOFs was recently proposed.[125] The aim was the encapsulation of enzymes to form a new generation of MOF-biocatalysts with long-term stability. The authors reported that hydrogen bonds between melamine and salicylic acid in the presence of well-distributed Zn^{2+} generate a 3D Zn-hydrogel network, which further coordinates with organic linkers (**Figure. 6**).

After the elimination of the hydrogel template, a well-defined micro- and mesoporous Zn-based H-ZIF-67 structure was obtained, containing pores in the range of 16-27 nm wide. Next, the enzymes glucose oxidase and horseradish peroxidase were successfully encapsulated and stabilized within the mesoporous ZIF-67 network, exhibiting broader operational stability and enzymatic activity, with respect to the bulk enzymes or the use of standard microporous MOFs (42-88 % *vs.* 14-54 % conversion).

Figure 6. Ordered mesoporous ZIF using melamine-salicylic acid coordinating agents. Reproduced with permission.[125] Copyright 2019, Wiley.

4. Synthesis of hierarchical MOFs assisted by hard-templating

4.1 Polymers

The use of soluble polymers for the generation of mesoporosity in microporous MOFs has been previously introduced in the last section, when considering the use of PVP as a template. Another example where polymers act as meso-/macro-structure directing agents is the one-pot HKUST-1 MOF crystallization in the presence of a precipitated polyvinylidene fluoride-based polymer. This combination generates a hierarchical macro-meso-microporous structure in the final polymer-MOF composite. The authors claimed that the framework instability created during the MOF growth as a result of MOF-polymer interactions is the driving force for the creation of a multi-pore HKUST-1 (with pore sizes range from 50 nm to 3 μm) as evident from the mercury intrusion porosimetry characterization.[126] Both HKUST-1 and polymer matrix are highly compatible showing no phase segregation, i.e. bulk polymer or MOF. The porosity of the MOF/polymer composite was confirmed by N_2 physisorption analysis, revealing a BET area of 527 $m^2 \cdot g^{-1}$ and a pore volume of 0.3 $cm^3 \cdot g^{-1}$. The study concluded that the expected microporosity of the MOF is preserved without being blocked by the penetration of polymer chains. In fact, a hysteresis loop at a high relative pressure confirmed the mesoporosity of the composite, which has an isotherm that is distinct from Type I (typical of microporous HKUST-1). This textural analysis further indicated the presence of mesopores in the composite material. In particular, mesopores in the range of 4 nm and 12 nm were deduced from the pore size distribution, employing the Barrett-Joyner-Halenda (BJH) method (entry 32 in Table 1).

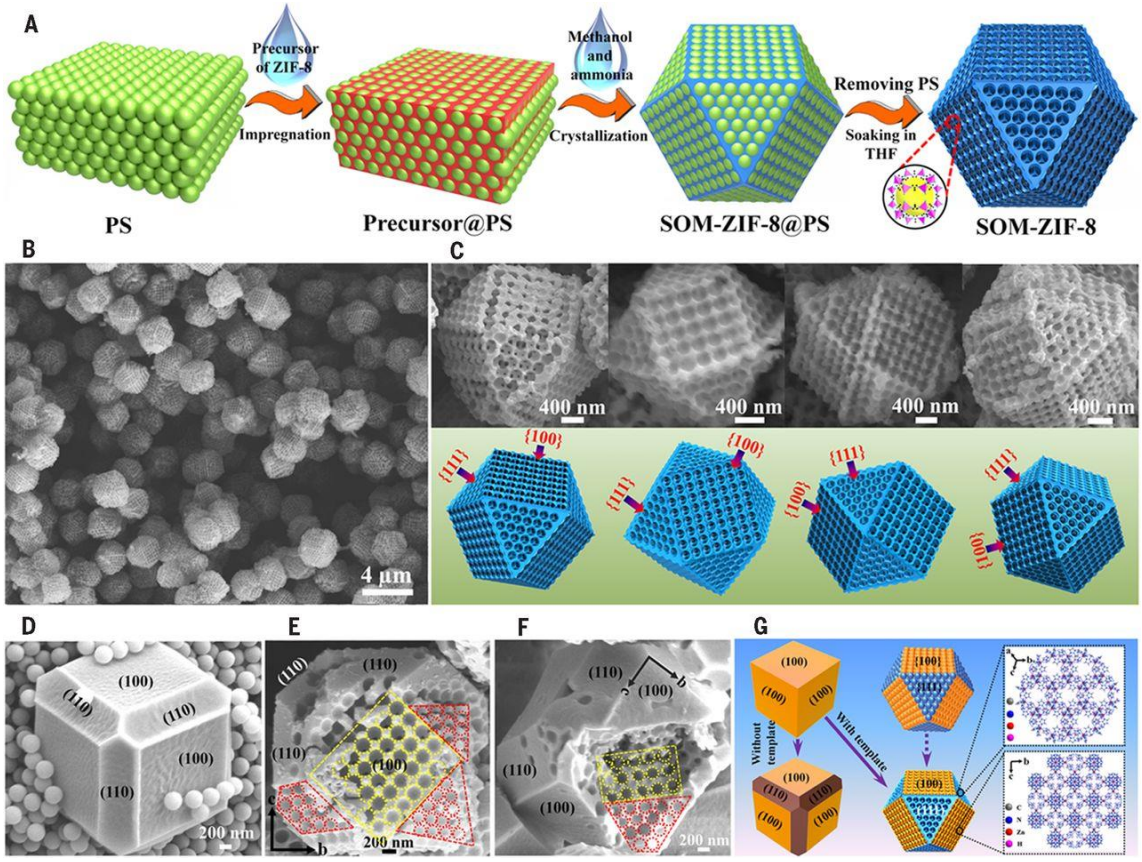

Figure 7. Schematic diagram of SOM-ZIF-8 (A). SEM image of SOM-ZIF-8 (B), individual crystals (C), ZIF-8 grown on the external surface of the PS template (D) and oriented growth within ordered voids (E and F). Illustration of the shaping and templating effects of the 3D-ordered PS template (G). Reproduced with permission.[127] Copyright 2018, Science.

3D ordered macrostructures with micropores forming the single-crystalline ZIF-8 structure were recently described (**Figure 7**). The use of polystyrene nanospheres as templates for the creation of macropores allowed the in situ macro-meso-ZIF-8 growth, containing ordered voids within a single crystal (with sizes of approximately 270 nm).[127] TEM images of the resulting hierarchical material indicated the presence of macropores, while selected-area single-crystal electron diffraction patterns confirmed the periodic nature of the pores within a single crystal. No domain boundaries or interfaces were observed. The improved catalytic activity in the Knoevenagel condensation of benzaldehyde with bulky groups indicated the facilitated mass transport within such hierarchical MOF, outperforming the polycrystalline hollow ZIF-8 having disordered macropores.

Another synthesis of defective ZIF67 (named DP-ZIF67) was based on the combination of PVP metallophilic polymer with the ZIF67 building blocks.[128] During the MOF crystallization, the polymer induces the disruption of imidazole-Co(II) bonds and generates mesoporous DP-ZIF67 crystals,

as seen in the different coordination environments of Co in the presence of PVP. TEM images of DP-ZIF67 showed the presence of large open and randomly distributed mesopores (20-40 nm). Those were also deduced by the Barrett–Joyner–Halenda (BJH) size distribution plot (entry 33 in Table 1). This catalytic platform showed potential multifunctionality, i.e. metal site catalysts and biocatalysts within a single MOF crystal. This platform promotes distinct cascade reaction steps, e.g. in a tandem mode, consisting of nucleophilic addition, chiral center generation, racemization and kinetic resolution, affording optically pure nitroalcohol derivatives in quantitative yields (**Figure 8**).

To finalize this section and introducing the next one, we briefly comment on how to construct hierarchical pore architectures in MOFs with the help of functional nanoparticles. By dissolving MOF encapsulated polystyrene spheres (PSS) in methanol, a controlled macropore/micropore ratio in ZIF-8 can be achieved.[129] After etching of the PSS, Pt nanoparticles can be introduced into the micro/mesoporous structure of cheese-like crystalline ZIF-8. The as-prepared Pt/M-ZIF-8 promotes the one-pot two-step Knoevenagel condensation-hydrogenation tandem process. While the macroporosity and basic sites favors the first step (passing from 87% to 97% conversion and from 0.016 h^{-1} to 0.027 h^{-1} rate constant upon introduction of macroporosity), the presence of hydrogenating metal nanoparticles promotes the subsequent hydrogenation step, without affecting the crystalline structure of hierarchical Pt/M-ZIF-8.

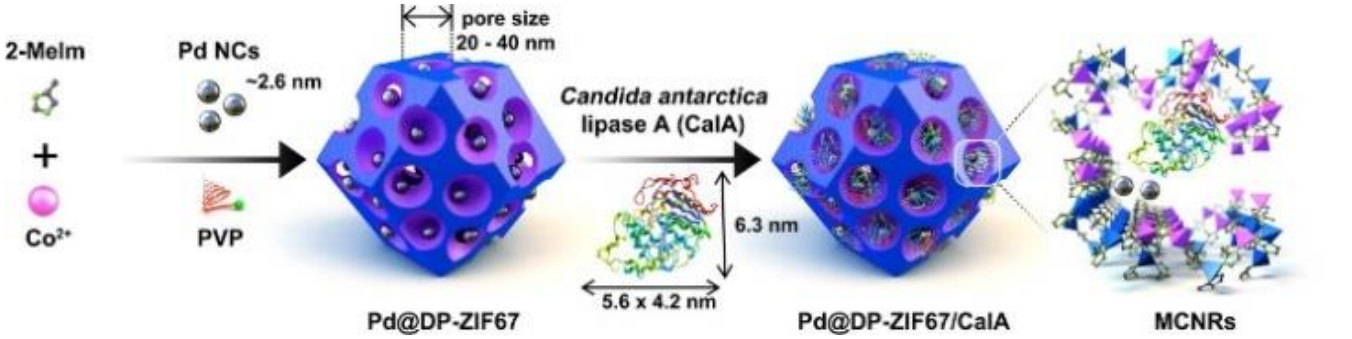

Figure 8. Incorporation of nanoparticles and biocatalysts in mesoporous ZIF-67. Reproduced with permission.[128] Copyright 2020, Wiley.

4.2 Metal nanoparticles

Meng et al. reported a straightforward approach to prepare hierarchical architectures in a series of NPs@MOFs by taking advantage of the thermal instability of defects around the nanoparticles in the interior of the pores.[130] Therefore, the nanoparticles act as templates at the core of the MOF particles, generating mesopores around the internal nanoparticles and maintaining the external MOF shell intact. Interestingly, one can control the dispersion of mesopores by positioning the nanoparticles at well-defined sites within the framework in order to optimize its catalytic performance. For example, hierarchical Pt@UiO-66-NH_2, Pt@UiO-66, Pt@ZIF-8, and Au@ZIF-8 have been reported after annealing at 250, 320, 300, and 330 °C, respectively. These mesoporous MOF catalysts were employed in the hydrogenation of olefins, exhibiting high reaction rates in contrast to the microporous MOFs.

Another simple and efficient method to construct hierarchical porosity and simultaneously functionalize the pores with sulfonic acid, was based on a palladium-reduction induced strategy.[131] The mesoPd@NUS-6 shows a surface area increase in line with the Pd loading: e.g. 5.0 wt% (426 m^2 g^{-1}) > 3.0 wt% (374 m^2 g^{-1}) > 1.0 wt% (334 m^2 g^{-1}). The mesopore generation mechanism is due to hydrogen bonding network NP-based destruction, as confirmed by two-dimensional 1H DQ-SQ MAS NMR. Thus, the Pd content inside the MOF is a straightforward manner to control the MOF mesoporosity. The adsorption capacity of the resulting mesoPd@NUS-6 was much higher than the microporous one, boosting the catalytic activity towards the dye molecule adsorption and olefin hydrogenation. In contrast to the a priori lower stability of mesoporous materials respect to microporous ones, the mesoPd@ NUS-6 is chemically stable and can be reused in several reaction cycles.

4.3 Metal-organic polyhedra (MOP)

Hierarchical UiO-66 was synthesized via a one-step or two-step process using MOF-5 as a template, due to its low hydrolytic and acid stability.[132] Indeed, direct exposure of MOF-5 in water or acid solution results in structural collapse and decomposition. On the contrary, UiO-66 is robust in acidic solution. Taking advantage of their relative differences in stability, hierarchical UiO-66 could be synthesized by leaching out MOF-5 template. Based on a two-step reaction process, MOF-5 particles with a size range of 370-520 nm were prepared and dispersed in DMF containing $ZrCl_4$ and BDC linker. The synthesis solution was thermally heated to produce MOF-5@UiO-66. The recovered solids were washed with HCI acid aqueous solution to obtain hierarchical UiO-66. The collected XRD pattern only revealed the typical fingerprint for UiO-66. The crystalline peaks of MOF-5, however, were not detected in the collected XRD pattern, which questions the presence of MOF-5 in the as-synthesized sample. According to the pore size distribution, UiO-66 with a mesopore size of ca. 11 nm was prepared. These mesopores are indeed much smaller than the particle size of MOF-5. Thus, one can directly rule out the role of MOF-5 as a template. Further elemental analysis showed that the added MOF-5 is not the actual template, instead, it was degraded and formed MOP in the DMF solution. These newly formed MOP thus act as the template to direct the formation of MOP@UiO-66 via decomposition and/or rearrangement of MOF-5 in the synthesis solution. Based on this discovery, other complex molecules and MOP, were used as

templates for the preparation of hierarchical UiO-66, ZIF-8 and DUT-5. Importantly, the mesopore size of the synthesized hierarchical MOFs by this approach could be adjusted according to the concentration of MOP. The advantage of having mesopores in UiO-66 was demonstrated for the uptake of large molecules with different sizes, such as Direct Blue 86 (4 × 12 × 14 Å), MOP-OH (40 × 40 × 40 Å) and bovine serum albumin (140 × 40 × 40 Å).

5. Stacking of nanoparticles (SN)

MOFs can adopt a hierarchical porosity via nanoparticle stacking by modulating the crystallization kinetics during MOF nucleation and growth processes to achieve nanosized (≤ 100 nm in diameter) MOF crystals. Meso- and/or macroporous structures of hierarchical MOFs constructed from nanoparticle aggregation are often defined as disordered interparticle voids. This type of hierarchical pore system is deferred from the meso- and/or macrostructures formed in a single MOF crystal. The formation of a critical number of nuclei is followed by a second particle growth termination after the consumption of the MOF precursors. Such LaMer model is key towards the formation of MOF nanoparticles, e.g. via direct precipitation modulated synthesis, microwave synthesis and CO_2 directed synthesis. At high MOF concentration reaching the critical limiting supersaturation threshold, MOF nanoparticles tend to aggregate into large agglomerates when dispersed into various solvents such as DMF or methanol.

Direct precipitation at room temperature followed by immediately quenching at -196 °C to limit the further crystal growth and solvent removal via a lyophilisation, has also been proven to be an efficient protocol to synthesize HKUST-1 and HPA@HKUST-1 nanocrystals.[133, 134] H4 type hysteresis loops in the relative pressure range from 0.50-1.00 corresponds to the mesopores generated via close packing of nanocrystals. The HKUST-1 and HPA@HKUST-1 nanomaterials outperformed their micron-sized counterparts for catalyzing methanolysis of styrene oxide and esterification of acetic acid with 1-propanol at low temperature, respectively. This confirms the advantage of shortening the diffusion pathway in liquid phase catalysis as a proof of concept for the first time in MOF catalysis. Close packing of nanosized HKUST-1 particles to form mesopores/macropores with a pore diameter ranging from 26-72 nm according to the BJH pore size distribution were prepared by the modulated synthesis method, where acetic acid and triethylamine were added in the synthesis mixture as modulators to inhibit crystal growth.[135]

Alternatively, HKUST-1 MOFs having large mesopores (13-23 nm) as evident from BJH pore size distribution curves were synthesized by using liquid CO_2 as a solvent. [136] Via this one-step approach, CO_2 accelerates the formation of HKUST-1 from Cu(II) salt and 1,3,5-benzenetricarboxylates (BTC), owing to the viscosity-lowering effect of CO_2, while the final solids were recovered through CO_2 extraction. The formation of mesopores was induced through spontaneous nucleation of HKUST-1 nanoparticles accelerated under the reduced solvency and viscosity of solvent due to CO_2 expansion at high CO_2 pressures. These nanocrystalline building blocks are assembled to form a continuous network as induced by the higher surface energy of nanoparticles. As a result, HKUST-1 with tunable mesoporosity and interparticle wall thickness was achieved by controlling the CO_2 pressure. Higher CO_2 pressure (2.0 MPa) is favorable to the formation of HKUST-1 with larger mesopores (10 nm) and thinner pore walls. At a higher CO_2 pressure (4.5 MPa), highly porous HKUST-1 with thinner mesopore walls was synthesized. At high CO_2 pressure of 6.6 MPa, the synthesized HKUST-1 has the largest mesopore sizes ranging from 20-30 nm with a diameter of the pore walls of ca. 10 nm. The assembly of HKUST-1 nanocrystals is less dense at higher CO_2 pressure due to the greater expansion of the solvent. The HKUST-1 with large intercrystalline mesopores and thin mesopore walls are formed once the CO_2 is evacuated. Despite the BET (Brunauer, Emmett and Teller) area of HKUST-1 synthesized via this approach is lower (BET area = 700 $m^2 \cdot g^{-1}$) in comparison to microporous HKUST-1 (BET area = 1200 $m^2 \cdot g^{-1}$) possibly due to pore interpenetration. A high total pore volume (>1.28 $cm^3 \cdot g^{-1}$) is achieved for the hierarchical HKUST-1. The as-synthesized hierarchical HKUST-1 was active for catalyzing the aerobic oxidation of benzylic alcohols at moderate temperature and low pressure (760 mm Hg) with added 2,2,6,6-tetramethylpiperidine-1-oxyl (TEMPO) as a co-catalyst. The hierarchical HKUST-1 with large interparticle mesoporosity showed superior catalytic performance, achieving 100% conversion of benzyl alcohol to benzaldehyde in 3 h with >99 benzaldehyde selectivity. The mesoporous MOF outperformed the commercial HKUST-1 (10% conversion in 3 h) under similar experimental conditions. More importantly, the hierarchical HKUST-1 showed no leaching of Cu(II) in the reaction mixture and was reusable up to four cycles, confirming the excellent stability and heterogeneous nature of the catalyst.

Hierarchical Zn-MOF-74 was synthesized from direct precipitation of zinc acetate and 2,5-dihydroxy-1,4-benzenedicarboxylate in DMF.[137] Zn-MOF-74 with disordered mesostructures in a continuous phase, having diameters in the range 5–20 nm, were formed via stacking of ultra-small nanocrystallites of 8.9 nm (entry 34 in Table 1). It shall be noted that only zinc acetate can be used as the only salt to synthesize such ultrasmall MOF-74 nanoparticles while other metal salts such as zinc chloride, and zinc nitrate were unsuccessful. A large dye molecule, Brilliant Blue R-250 (BBR-250) was used as a molecule to probe the accessibility and adsorption capacity of hierarchical MOF-74, in comparison to its parent microporous counterpart. BBR-250 has a molecular dimension of ~1.8 nm × 2.2 nm which is larger than the micropore size of the parent MOF-74. The adsorption studies revealed that the hierarchical MOF adsorbed BBR-250 up to 17.9%, whereas the parent microporous MOF-74 only adsorbed 2.7% via external surface adsorption. These results confirmed the advantages of the creation of secondary mesopore structures in a microporous solid to allow access of large molecules to less coordinately saturated surface metal centers. M–MOF-74 (M=Mn, Co, Ni, Cu, or Zn) nanomaterials were synthesized via this approach and evaluated as catalysts for the conversion of cyclohexene employing peroxides as oxidizing agents.[138, 139] The nanocrystalline MOF-74 catalysts showed superior catalytic activity than their micrometer-sized homologs. However, it shall be noted that leaching of metal was also observed, indicating the chemical instability of this particular MOF for liquid phase catalysis.[139] Nevertheless, the ~1 nm pores of

standard M-MOF-74 (M=Mn, Co, Ni, Cu, or Mg) served as active and stable redox-active host of confined $Pd(OAc)_2$ and tert-butyl hydroperoxide species with high performance in the heterogeneous version of the Fujiwara-Moritani reaction. Higher pore size is found in MOF-808 (close to 2 nm), which shows an optimal catalytic performance in the above mention oxidative coupling, and in the post-synthetic functionalization with amino acids for organocatalytic applications. [140-142]

Modulated-mediated synthesis using a mixture of acetic acid and hydrochloric acid added to the synthesis reagents has also been employed to synthesize UiO-66 xerogel constituting of crystalline MOF nanoparticles with particle sizes range from 10 to 15 nm.[143] The UiO-66 xerogel exhibits uniform mesopores of ca. 15 nm in diameter according to the BJH method. The calculated pore volume and BET area were 2.09 $cm^3 \cdot g^{-1}$ and 1459 $m^2 \cdot g^{-1}$, respectively for the air-dried UiO-66 xerogel sample (entry 35 of Table 1). A modification of this method with a control drying process at room temperature was described by Fairen-Jimenez and co-workers, which successfully transformed this UiO-66 gel into sub-mm-sized UiO-66 monoliths (**Figure 9**).[144] The N_2 sorption revealed a Type IV isotherms with a steep uptake of N_2 at low relative pressure (P/P_o = <0.1) signifying the presence of microporosity and a hysteresis loop ascribed to mesoporosity.[134] By varying the solvent used for washing as well as the drying temperature, macroscopic UiO-66 monoliths with tunable mesoporosity could be prepared, as evident from the BJH analysis. The observed mesoporosity in the monolithic macrostructure corresponds to the interparticle void space formed from the densification of the 10 nm primary MOF particles. The role of the drying temperature in the monolith formation was investigated through drying the MOF gel at different temperatures (100 and 30 °C) after washing with ethanol. The results obtained showed that high drying temperatures (100 °C) induce interstitial spaces formation in between the nanoparticles as a result of fast solvent elimination from the MOF gel, destroying the gel networks which give rise to a powder.

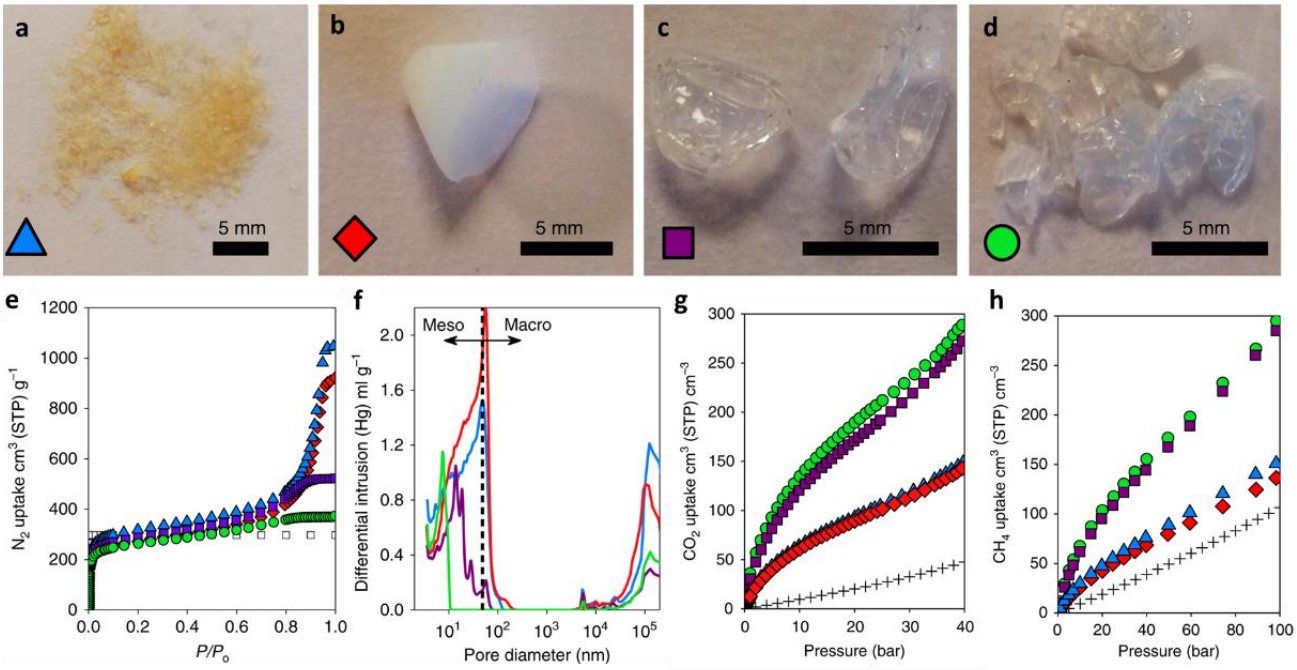

Figure 9. a) UiO-66 gel washed in ethanol and dried at 200 °C, b) UiO-66 gel washed in ethanol and dried at 30 °C, c) UiO-66 gel washed in DMF and dried at 30 °C, d) UiO-66 gel washed in DMF with extended centrifugation and then dried at 30 °C. e) N_2 adsorption isotherms, f) Hg-porosimetry pore-size distributions of UiO-66 monoliths and the respective g) volumetric CO_2 absolute adsorption isotherms and h) volumetric CH_4 absolute adsorption isotherms measured at 298 K. Reproduced with permission.[144] Copyright 2019, Nature.

On the other hand, centimeter-sized opaque monoliths were obtained by drying the MOF gel at 30 °C, supporting the proof-of-concept importance of drying temperature in controlling the formation of macroscopic MOF monoliths. The influence of washing solvent on the monolith density was also investigated by washing the MOF gel with DMF instead of ethanol before drying at 30 °C. This step led to optically transparent UiO-66 monoliths with improved mechanical stability and bulk density. When solvents with varied boiling points were used for MOF washing, the monolithic MOFs obtained demonstrated different optical properties, illustrating the complexity of solvent mediated interactions with the MOF nanoparticle in a gel. Previous studies explained that solvent with slow evaporation rate (e.g. DMF) would facilitate primary particle interaction and enable both primary particle densification which directly influences the micro-/mesoporosity ratio. The UiO-66 monolith with the highest micro-/mesoporosity ratio of 0.85 exhibited a total gas adsorption for both and CO_2, significantly higher than the bulk microporous UiO-66. Computational simulations showed that the monolithic sample with high microporosity would facilitate a moderate uptake of CH_4 at low pressures while mesopores enhanced gas condensation at higher pressures. These results highlight the importance of micro- and mesoporosity correlation in optimizing CH_4 uptake.

6. Top-down engineering of hierarchical MOFs: towards defect engineering

To efficiently prepare MOFs with entrapped voids in the mesoporous range, we have described several in situ solvothermal self-assemble methods that produce, for instance, hollow structured polycrystalline MOF spheres after removal of sacrificial templates. However, open frameworks and metal sites formed in (defect-engineered) MOFs during bottom-up solvothermal self-assembly or layer-by-layer growth syntheses methods still have limitations.[80, 145] In this section, we will highlight the controlled crystal etching as a typical top-down approach suitable for creating voids inside solids, like MOFs, where the molecular control of the etching allows for the generation of hierarchical porosity. Thus, instead of growing mesoporous MOFs using large linkers and/or templates under certain reaction conditions (bottom-to-top approach), we start from preformed defect-free MOFs and generate mesoporosity within the MOF crystal via post-etching treatments (top-down approach).

6.1 Acid leaching

The acid leaching approach was first introduced by Wee *et al.* in 2013 for the preparation of hierarchical ZIF-8 nanocrystals.[146] Secondary mesoporosity was generated in ZIF-8 nanocrystals during the esterification of oleic acid with glycerol in *tert*-butanol at 150 °C. TEM images revealed small cavities inside individual ZIF-8 nanoparticles, which ranges from 5 to 10 nm in diameter. The hierarchical pore system of ZIF-8 nanocrystals achieved via acid leaching was also confirmed by a Type IV N_2 sorption isotherm. This technique is similar to hierarchical zeolite synthesis where acid or base is used to leach out aluminum or silicon, respectively, from the zeolite structure. This post-synthetic modification process is known as dealumination or desilication in the zeolite field.

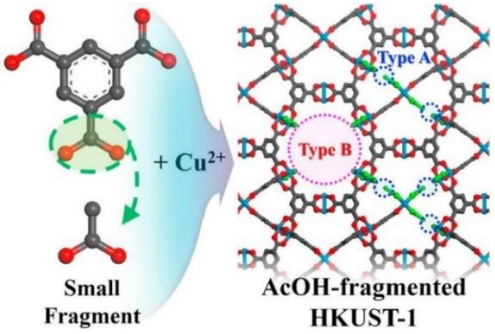

Figure 10. Blue region: Type A site formed by missing a BTC linker; Pink region: Type B site created by missing a Cu paddle-wheel cluster and four BTC linkers. Reproduced with permission.[147] Copyright 2018, Elsevier.

The water-sensitive HKUST-1 MOF was tuned to favor the molecular transport of substrates via defect engineering using acetic acid promoted etching (known as "fragmented linker" co-assembly). This strategy generates micro and, more important, mesoporous defects (2-15 nm), thus improving the surface area and total pore volume of the microporous HKUST-1.[147] An optimal acetic acid amount is needed since an excess of AcOH (> 0.3 mL), results in large mesopores (> 25 nm) instead of the formation of small mesopores (between 2-15 nm). Two types of structural defects were created based on either BTC linker or copper paddle-wheel cluster removal (**Figure 10**). The porosity of the defective frameworks originating from both defects was found to increase, suggesting that the acetic acid-fragmen

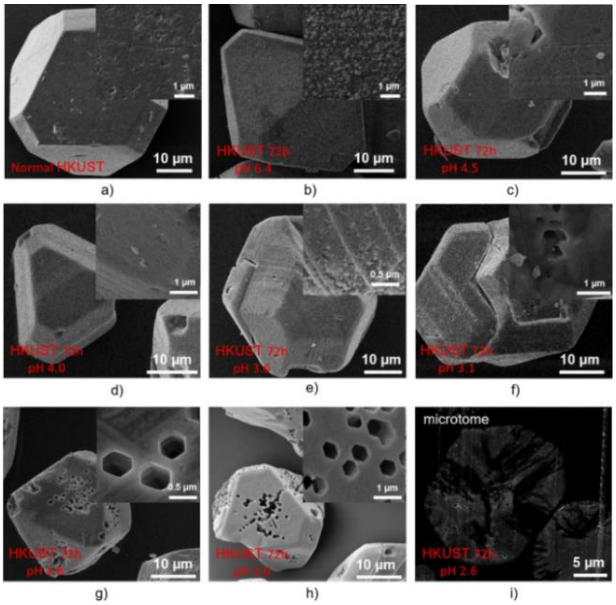

Figure 11. SEM images of HKUST-1 etching in phosphoric acid using DMSO and MeOH as dilute solvents at different concentrations. Reproduced with permission.[148] Copyright 2019, Nature.

tation strategy is an efficient approach towards the generation of a hierarchical MOF with tailored pore properties.

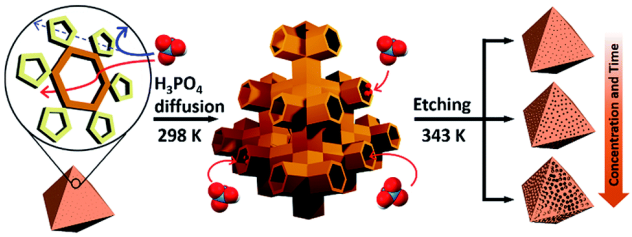

Figure 12. Left: MIL-100(Fe) crystal with hexagonal and pentagonal windows; middle: acid diffusion into tetrahedral channels through hexagonal windows; right: resulting mesopores after etching. Reproduced with permission.[149] Copyright 2017, Royal Society of Chemistry.

Another study employs phosphoric acid promoted etching in dimethyl sulfoxide and methanol.[149] The weight loss of sample etched depends on the concentration of the acidic solution (pH 2.6) and treatment time (10 days) for the creation of macroporous holes (0.5 µm) in HKUST-1. The final HKUST-1 microstructure (d = 0.83 nm) and external crystal morphology were preserved (**Figure 11**). According to TG analysis, structural defects are generated in the etched HKUST-1 sample by losing one copper cluster and four BTC linkers. The leaching of the molecular building blocks via-phosphoric acid treatment was proposed as the main mechanism responsible for defect formation in HKUST-1. H_3PO_4-promoted etching of the HKUST-1 framework eventually results in the loss of the molecular building blocks that leads

to lower BET surface areas. The amount of disassembled clusters and linkers is proportional to the H_3PO_4-etching time, although the crystallinity of the MOF is maintained due to the acid inaccessibility to the majority of the molecular building blocks.

A simple etching-based method to create mesopores in the iron MOF MIL-100, $Fe_3(\mu_3\text{-}O)(H_2O)_2(OH)(BTC)_2$, was recently reported by Koo et al.[149] The penetration of phosphoric acid molecules in the MOF windows that has adequate size-selective dimensions (0.89 nm x 0.49 nm) results in the partial etching of both metal and linkers near the windows, generating larger cages (**Figure 12** and **13**). It is worth mentioning that, as reported for the previous example of HKUST-1, after gradual etching at 70 °C most of the microporous cages are preserved as well as the crystallinity and particle morphology. The collected N_2 sorption analysis of the etched MIL-100 sample revealed a typical isotherm with a H1 hysteresis loop, indicating the generation of ordered mesoporosity. The BET area of the hierarchical material was reported to be 750 $cm^3 \cdot g^{-1}$, with a mesopore volume of 1.15 $cm^3 \cdot g^{-1}$. According to the Barrett–Joyner–Halenda (BJH) analysis, the observed hysteresis loop corresponds to mesopore sizes in a range from 2.4 to 18.4 nm, depending on the etching time for a particular acid concentration.

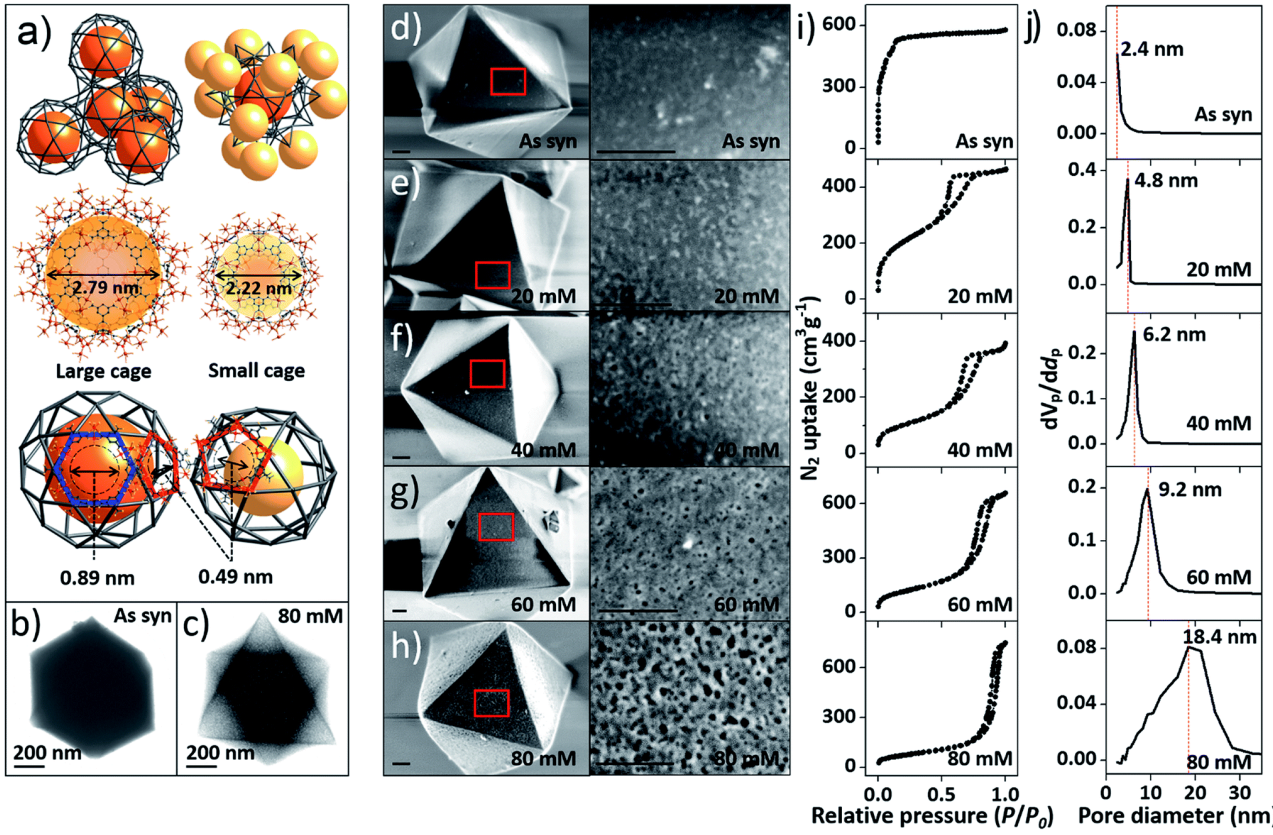

Figure 13. (a) Top-left: tetrahedral geometry constructed by large cages; top-right: a large cage surrounded by 12 adjacent small cages; middle: structures of the large and small cages; bottom: hexagonal and pentagonal windows. (b and c) TEM images of pristine MIL-100(Fe) and MIL100(Fe)-80. (d–h) SEM images of pristine and acid-etched MIL-100(Fe) (scale bars: 200 nm), (i) N_2 sorption isotherms (at 77 K) and (j) pore size distribution profiles of as-synthesized MIL-100(Fe) and MIL-100(Fe)-20, 40, 60 and 80 mM H_3PO_4-treated. Reproduced with permission.[149] Copyright 2017, Royal Society of Chemistry.

These methods highlight the possibility of a simple mesopore generation with inexpensive mineral acids, such as acetic or phosphoric acids. Although it is often possible to control the mesopore range, this type of top-down approaches lack from the molecular precision of SBU/linker design (see linker extension in section 2). Indeed, it is difficult to precisely tune the pore size of the final hierarchical MOF with less than 2 nm precision (at the microporous domain). Besides, the crystallinity of the MOF is often compromised under low pH, and the method is not applicable to a broad range of (labile) topologies. The ideal tuning of mesoporosity needs for simplicity and precision, together with the use of economic synthetic methods, which will be achieved by further controlling the acid-SBU interactions during the etching process.

In an innovative approach, MOFs having large pores with tunable sizes were obtained via the use of the so called "prolabile linkers approach". This consists of (partial) disconnection of some of the relatively unstable metal-linker bonds with the help of acid etching, named as "linker labilization". This is a controlled pathway for the induction of missing-linker defects. The concept has been demonstrated for labile 4-carboxybenzylidene-4-aminobenzoate linkers in a Zr-MOF known as PCN-160, which reduced the connection number of Zr_6 clusters after partial removal of the linkers.[150] The removal of 25% of the linkers was determined by UV-Vis and ^{1}H-NMR techniques. Textural properties, such as

mesopore size and pore size distributions of PCN-160, can be precisely controlled by optimizing the exchange ratios and acid concentrations. However, an excessive acid etching gradually dissolves the materials, since the defect sites are less stable in the framework. In contrast, the parent material enlarges the mesopores while maintaining the crystallinity. Since the acid etching partially dissolves the MOF crystals from the inside out, the small mesopore volume decreases as the large mesopore emerges (enlarging the 2.5 nm mesopores).

The same strategy was applied to enlarge the mesopore size of a hierarchical MOF, known as CYCU-3. This material has mesoscale hexagonal channels with a pore opening of 3.0 nm interconnected via smaller trigonal pores of 1.5 nm in diameter. These large hexagonal channels are ideally suited for the encapsulation of Cytochrome c enzyme, with a molecular dimension of 2.6 nm x 3.2 nm x 3.3 nm, while the triangular channels facilitate substrate diffusion, e.g. phenylenediamine. However, these triangular channels are too narrow to allow fast diffusion of a bulky substrates, e.g. 2,20-azino-bis(3-ethylbenzothiazoline-6-sulphonic acid), between neighboring channels, resulting in lower catalytic activity. By replacing 22% of the AZDC (azobenzene-4,40-dicarboxylate) linkers with labile CBAB linkers, attempted for the synthesis of CYCU-3 and subsequent leaching of the labile linkers with diluted HCl in DMF, the mesopores of CYCU-3 can be enlarged to 7 nm as evident from N_2 sorption analysis and the respective pore size distribution. CYCU-3 with larger mesopores showed an improved activity for the oxidation of the bulky 2,20-azino-bis(3-ethylbenzothiazoline-6-sulphonic acid), highlighting the importance of a hierarchical porous structure with mesopore sizes large enough for the efficient substrate diffusion between neighboring channels.

6.2 Thermolysis

Zhou and co-workers reported a thermolysis approach for creating hierarchical pores in a series of microporous MOFs.[151] This approach relies on the pre-synthetic installation of thermally less stable organic linkers into a stable MOF. For example, a multivariate UiO-66 was synthesized from thermostable (e.g. BDC) and thermolabile (e.g. BDC-NH_2) linkers. By controlling the decomposition temperature at 350 °C, the thermolabile linker losses its carboxylic group and is thus selectively removed from the framework (**Figure 14**), as confirmed by TGA-MS results showing CO_2 was the only gaseous product detected upon evacuation of the trapped solvents. The decarboxylation process was also supported by in situ infrared spectroscopy and ex situ X-ray photoelectron spectroscopy. The COO^-/Zr ratio was found to decreases from ~41% to ~25% after linker thermolysis at 350 °C for 3.5 h. Intriguingly, the pore size of UiO-66 can be systematically tuned from 1.2 to 15 nm by controlled linker thermolysis while retaining the crystallinity and porosity. This represents an advantage over conventional acid-leaching methods, although both could in principle control the H^+ concentration or thermal energy needed for metal-linker dissociation.

In a demonstration of genericity, this approach is also applicable to create large mesopores in other multivariate MOFs with different metal clusters, such as MOF-5(Zn), MIL-53(Fe), MIL-125(Ti), and UiO-66(Hf). It should be noted that metal oxide nanoparticles, e.g. ZrO_2 with ultrasmall crystal sizes (1–3 nm), were simultaneously formed during the linker thermolysis process as evident from TEM imaging, giving rise to the production of a new bifunctional MOF catalyst. This hierarchical MOF composite catalyst (ZrO_2@UiO-66) showed high catalytic activity for Meerwein–Ponndorf–Verley (MPV) reaction, outperforming its parent microporous UiO-66 and ZrO_2 nanoparticles under similar reaction conditions. The demonstrated method is a breakthrough in the design of bi-functional MOF catalysts with enhanced Lewis acidity via homogeneous encapsulation of ultra-small metal oxide nanoparticles and unwinding the active metal sites. Therefore, the enhanced catalytic activity may not exclusively result from changes in porosity. The concomitant formation of more open (and exposed) Zr coordination sites as well as additional ultra-small metal oxide particles could play crucial role to achieve higher activities in such Lewis acid catalysis for transferring protons from alcohols to ketones.

Another recent publication by Fisher and co-workers demonstrated similar strategy to induce hierarchical pore system in Ru/Rh-HKUST-1 and its implication on ethene dimerization catalysis.[152] Similar to UiO-66, the respective Ru/Rh-HKUST-1 MOFs showed enlarged pore formation (>15 Å) as a result of micropore (~7–8 Å) merging due to removal of pore walls as a result of linker fragmentation via complete BTC elimination or partial BTC ligator site decarboxylation accompanied by the observation of ultra-small metallic rhodium nanoparticles upon thermal treatment at 250 °C. Defective Ru/Rh-HKUST-1 samples showed an enhanced ethane uptake with a gradual increase in ethane sorption enthalpies from 30 to 40 kJ mol^{-1}, possibly due to the induced open metal sites per paddlewheel cluster. The defective $Ru^{II,II}$-HKUST-1 catalyst was found more active than the defective RuRh HKUST-1, $Rh^{II,II}$-HKUST-1 and pristine $Ru^{II,III}$-HKUST-1 catalysts for ethene dimerization to 1-butene.

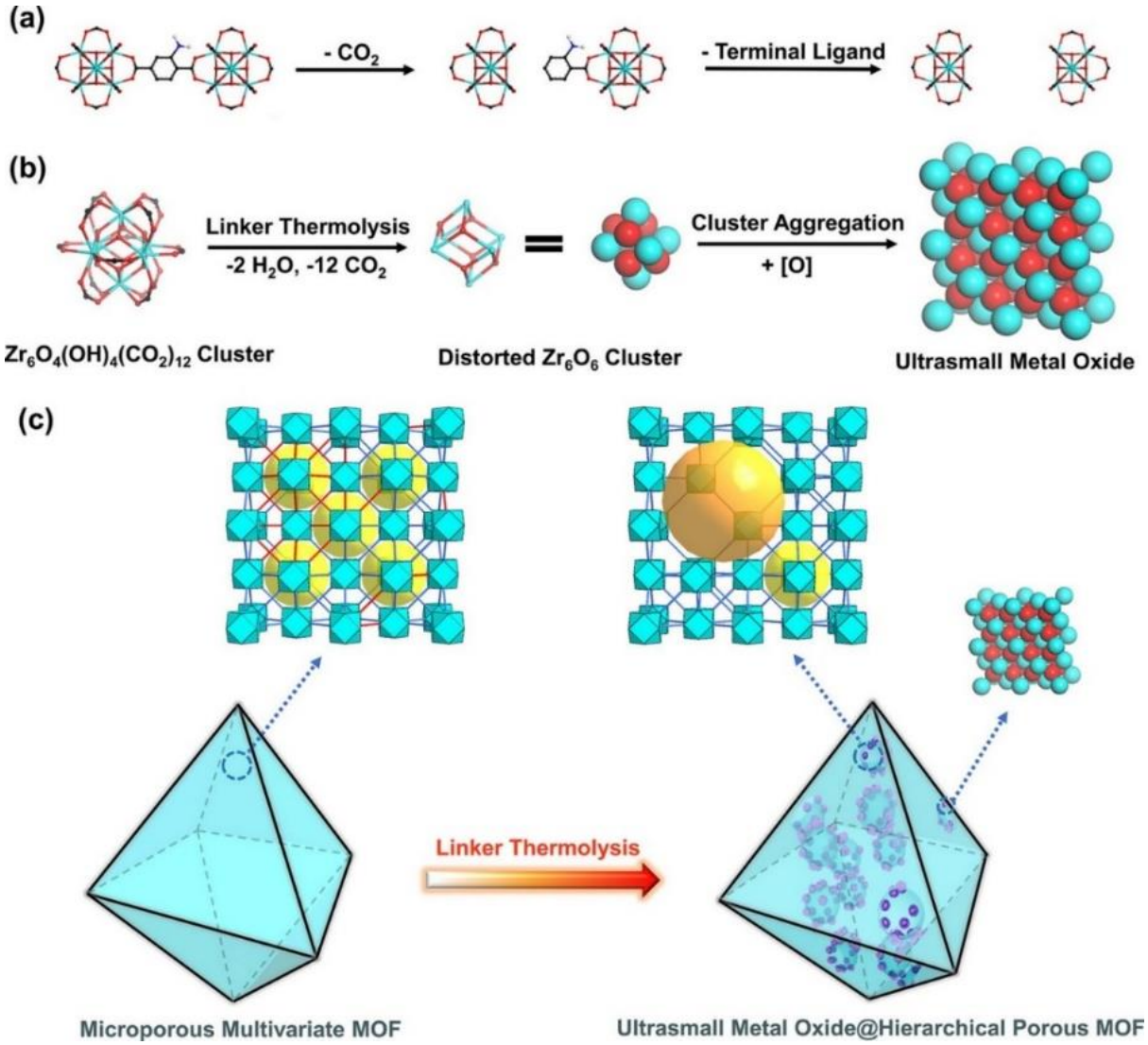

Figure 14. Mechanism of hierarchically porous structure formation. (a) The amino-functionalized linker tends to undergo a decarboxylation process under relatively low temperature, and the resulting terminal ligand could be further removed through thermal or chemical treatments. (b) $Zr_6O_4(OH)_4(CO2)_{12}$ clusters are transformed into decarboxylated Zr_6O_6 clusters after linker thermolysis, and they tend to aggregate with the assistance of oxygen species, forming ultrasmall MO nanoparticles eventually. (c) Overall, the microporous MTV-UiO-66-NH_2 is converted into ultrasmall MO@HP-MOF composites through controlled linker thermolysis. Reproduced with permission.[151] Copyright 2018, American Chemical Society.

6.3 Photolysis

Apart from heat treatment, Zhou's group also reported the use of a laser to create mesopores in UiO-66 through the dissociation of chemical bonds to remove photolabile linkers from a MOF structure.[153] In this case, a careful selection of the photolabile linker is essential, since otherwise the MOF will be transformed into metal oxides, transition metal carbides or alloys under laser radiation. A tetracarboxylic porphyrin linker TCPP (TCPP = tetrakis(4-carboxyphenyl)porphyrin) was selected to serve as the photolabile linker in the crystallization of UiO-66 in combination with traditional BDC linker, taking into consideration its strong adsorption at 405 nm. The multivariate UiO-66 was treated with a laser at 405 nm to allow fast and selective removal of photolabile linkers while preserving its crystalline structure. Pore size distribution showed the existence of 3 nm wide mesopores uniformly distributed over the UiO-66 crystals after laser treatment as a result of missing cluster defects. More importantly, the mesopore/micropore ratio can be tuned with the exposure time (entry 35 in Table 1). It shall be noted that washing of the laser-treated UiO-66 MOF with a DMF solution containing 0.1% HCl can further enhance its BET area and mesopore size in comparison to the unwashed sample. Using this approach, the mesopore size of UiO-66 can be further increased from 2 to 4.5 nm by incorporating a secondary photolabile BDC-NH_2 linker into the UiO-66-TCPP to induce lability in the stable UiO-66 structure, showing excellent homogeneity between these two photolabile linkers. According to TEM imaging, the formation of mesoporosities in UiO-66 via photolysis also causes roughening of crystal surfaces. In addition, ZrO_2 nanoparticles were formed, suggesting photo-induced cluster-cluster aggregation. A similar phenomenon was observed from thermolysis. This method is proven to be effective for the synthesis of other hierarchical multivariate MOFs such as UiO-66-Cu-

TCPP, UiO-66-Co-TCPP, ZIF-8(Zn)-TCPP, UiO-67-TCPP, and UiO-66(Hf)-TCPP, indicating a genericity of the method.

6.4 Hydrolysis

In addition to thermolysis and photolysis, hydrolysis has also been introduced by Kim and co-workers to generate secondary mesopores in microporous MOFs. A microporous MOF namely POST-66 (POST= material of Pohang University of Science and Technology), was synthesized and transformed into a hierarchical POST-66 by simple water treatment.[154] This approach generated POST-66 with bimodal mesopores of 3.8 and 13.9 nm in diameter, as evident from the BJH pore size distribution while keeping the original microporous structure partially intact (entry 38 in Table 1). The obtained sorption isotherm revealed an H1 type hysteresis loop, ascribed to its ordered cylindrical pores. The total pore volume was found to increase from 0.89 to 0.94 $cm^3 g^{-1}$, while the BET area decreases significantly from 2400 to 620 $m^2 g^{-1}$, due to the partial degradation of the microcrystalline structure to enable mesopores formation during hydrolysis. The pore volume ratio of micro-/mesoporosity can be systematically tuned by the manipulation of hydrolysis time and temperature.

According to ICP-AES and UV/Vis spectroscopy, the creation of mesopores in POST-66 was attributed to the leaching of yttrium ions (ca. 19%) when treated in water for less than 1h. However, no leaching of HMTT (methyl-substituted truxene tricarboxylic acid) linker was detected during the water treatment. The authors proposed a two stages mechanism for the transformation of micro- to mesopore in POST-66 upon water treatment. The yttrium ions were first dissociated from the structure, which leads to the generation of secondary mesopores with a mesopore size of 3-4 nm associated with a reduction in its microporosity. In the second stage, reassembling of yttrium ions and HMTT ligands at the defective sites was observed, leading to a large mesopore size of 10 nm. New amorphous phases were formed simultaneously at the mesopore mouth to stop further leaching of yttrium ions, as indicated by no further loss of yttrium after 1 h. The hierarchical POST-66 having large mesopores was used as a host to encapsulate large guest molecules such as proteins and enzymes (such as vitamin B12, cytochrome c, myoglobin, and horseradish peroxidase). For example, horseradish peroxidase encapsulated in the hierarchical POST-66 showed a superior catalytic activity for co-oxidation of 4-aminoantipyrine and phenol to N-antipyryl-p-benzoquinoneimine at room temperature, achieving 78% conversion of 4-aminoantipyrine. Under similar reaction conditions, the hierarchical POST-66 showed no catalytic activity while the homogeneous horseradish peroxidase converted 93% of 4-aminoantipyrine. Filtration tests after 5 and 15 min showed no leaching of the enzyme from POST-66. This new MOF catalyst could be reused several cycles confirming the nature of catalyst integrity and heterogeneity. However, deactivation of the catalyst was noted after the fifth catalytic cycle.

Finally, we would make a comment on the use non-water stable MOFs for catalytic and adsorptive processes involving water. This is very much limited by their susceptibility to aqueous or vapor conditions. Nonetheless, this disadvantage can sometime turn into advantage where the instability of MOFs in aqueous conditions can be used to tune the functional active sites (e.g. Lewis/Brønsted acidity and/or open-metal sites) of the MOFs, including the generation of a secondary mesoporosity that play a crucial role in overcoming the diffusion limitations of the microporous solids, in particular for liquid phase catalysis and adsorption. It shall be noted that the use of MOFs as catalysts is still limited for low-temperature and/or non-aqueous catalysis, preventing their use in many important chemical processes involving high temperature and/or water such as hydrocarbon cracking or hydroisomerization reactions.

7. Conclusions and outlook

A plethora of procedures have been described in order to expand the porosity of the MOF from the micro to the meso and macro domain. However, all methods have in common a tendency to manipulate one or several parts of the reticular material (e.g. SBU, organic linker or void spaces) in order to extend or disconnect the building blocks in a controlled manner. This has been done, on the one hand, by carefully designing the appropriate building blocks (SBUs, use of extended linkers), starting with well-defined reagents that give rise to hierarchical porous architectures by self-assembly of the inorganic and organic units (bottom-up approach). On the other hand, by selecting the appropriate reaction conditions (e.g. temperature, time, concentration of precursors) one can generate different levels of hierarchy, controlling the dimensionality and porosity of the final material (top-down approach). While elongated linkers require an important synthetic and economic cost, the use of simple additives as structure-directing agents and crystal growth modulators containing acid or base functionalities, allows for the straightforward generation of porosity, e.g. modulated or templated approach.

In this sense, the use of hard templates has revitalized the area of molecular imprinting, rising up novel composite hierarchical MOF which maintains the porous structure after removal of the template. It is foreseen that limitations of this type of material, such as cost or stability, will be overcome in the near future by the use of novel SBUs that shows greater robustness. In general, stacking of MOF nanocrystals would result in ultra-large interparticle meso- and macroporosities of 26 and 72 nm, respectively. Hard and soft templating approaches often lead to the creation of large disordered mesostructures in MOF crystals up to 40 nm, followed by the top-down engineering of hierarchical MOFs induced via defect engineering approach which creates disordered mesopores range from 2.3 to 14.8 nm. The extended linker approach generates the largest ordered mesopores up to 6.7 nm (e.g. NU-1007), followed by the mixed-linker approach which produces MOF-210 having the largest open cage length of 4.8 nm.

Future endeavors should focus on exploring Earth-abundant metals that are inexpensive, biocompatible and biodegradable as well as the constitutive organic linkers. Biocompatible and biodegradable multifunctional hierarchical/mesoporous MOFs could potentially serve as hosts for the encapsulation of therapeutic drugs and act as theranostic platforms for delivering drugs to the targeting cells for effective cancer treatments. The concerns regarding the cytotoxicity of mesoporous MOFs for biomedical applications have recently been tackled by Horcajada and co-

workers.[155] MTT assays revealed that mesoporous MOFs, e.g. MIL-100(Fe), exhibit low toxicity values comparable to those of currently commercially drug delivery systems. Although at the present stage, imaging and therapeutic applications employing hierarchical/mesoporous MOFs are still in the embryonic stages, far from for clinical trials, molecular simulations could play a key role in providing compendious understanding at molecular-level to gain insights of the thermodynamics of adsorption-desorption in MOF as well as structural details of the drug-delivering processes to enable a fast screening for selecting the best performance hierarchical/mesoporous MOFs. Thus, we believe that a leap step can be made to push the development of hierarchical/mesoporous MOFs for clinical applications.

Overall, hierarchical MOFs with interconnected micro- and mesoporosities increase the uptake of gases at high pressure, while the hierarchical arrangement of micro/mesopore system facilitates the adsorption and separation properties. Hierarchical MOFs with large mesopores show great potential for the encapsulation of large substrate molecules such as organic dyes and enzymes in the liquid phase, which offers new avenues to improve biocatalysed processes. Functionalized hierarchical/mesoporous MOF catalysts outperform their homogeneous counterparts and parent microporous MOFs for organic synthesis due to the enhanced mass transfer rates between reactants and products. These types of catalysts can promote organic reactions involving large substrate molecules, which can never be achieved by their microporous counterparts with much narrow micropores.

Among all the discussed methodologies developed to design hierarchical/mesoporous MOFs, we are confident to conclude that the bottom-up modulator-induced defect-engineering is one of the most promising tool to create hierarchical pore systems in MOF catalysts, as it allows systematic tuning of the defect sites (i.e. Lewis and/or Brønsted acidity) which are essential for organic synthesis. Besides the discussed case studies in section 2.4, another recent studies by Feng and co-workers documented the preparation of a highly defective and yet stable UiO-66 MOF catalyst having up to maximum six defects per zircornium cluster, employing 4-sulfobenzoic acid potassium salt as the modulator.[156] The resulting catalyst showed superior catalytic activity, selectivity and chemical stability for catalyzing the isomerization of α-pinene oxide. This is a cutting-edge example of how to address the formation of open metal sites as structural defects in hierarchical MOFs, due to systematic missing of linkers, of particular interest to enhance host-guest interaction between the adsorbate and adsorbent for improving the adsorption related applications. Thus, the development of hierarchical/mesoporous MOF materials represents a new research horizon towards new multifunctional materials that outperform traditional microporous MOFs and state-of-the-art mesoporous materials such as ordered mesoporous organosilicas.[142, 157]

Although hierarchical/mesoporous MOFs have shown superior performance in catalysis and adsorption-related processes, outperforming its microporous counterparts and other porous materials, little attention has been given to MOF upscaling, production cost, stability and reusability. Moreover, hazard issues related to the use of DMF and methanol as common solvents for the synthesis/washing of MOFs need to be investigated in detail since in laboratory-demonstrated research, MOFs are often synthesized in milligram or gram scale, and the process may change the MOF properties upon scale-up. In view for future exploitation and commercialization of MOFs, the development of scalable, sustainable (water is preferred over organic solvents) and cost-effective synthesis processes (e.g. continuous-flow synthesis) is essential to meet a competitive cost price, able to compete with the conventional zeolite materials (which are priced 1-10 US dollars per kilogram).

Currently, MOFs are priced > 10 US dollars per gram by chemical companies worldwide, probably due to their small-scale MOF manufacture. Recent techno-economic analysis of MOF production performed by Veenstra and co-workers revealed the potential of producing MOFs (e.g. MOF-74) at a lower cost of < 10 US dollars per kilogram taking into consideration MOFs produced at a large-scale of 2.5 Mkg/year using linker and metal salt at a reduced cost price.[158] Nonetheless, the higher cost of MOFs shall not limit their potential industrial use as catalysts and adsorbents as MOFs with high performance (e.g. high adsorption capacity and selectivity) are also considered as an important cost driver too. With continuous research efforts towards these challenges, we are confident that hierarchical/mesoporous MOFs would contribute to improve the performance of future ordered porous solids in catalytic and adsorption processes relevant to society.

Corresponding Authors

francisco.c.garcia@uv.es
lhw31@cam.ac.uk

ACKNOWLEDGMENTS

F. G. Cirujano acknowledges the support of a fellowship from "la Caixa" Foundation (ID 100010434). The fellowship code is LCF/BQ/PI19/11690011. N. Martín acknowledges the "Juan de la Cierva formación" fellowship with code FJC2018-035455-I. L. H. Wee acknowledges the Fonds Wetenschappelijk Onderzoek-Vlaanderen for a senior postdoctoral research fellowship and International Mobility fellowship under the contract numbers of 12M1418N and V402319N, respectively.

REFERENCES

(1) Yang, X.-Y.; Chen, L.-H.; Li, Y.; Rooke; J. C., Sanchez, C.; Su, B.-L. Hierarchically porous materials: synthesis strategies and structure design. *Chem. Soc. Rev.* **2017**, *46*, 481-558.

(2) Sun M.-H.; Huang, S.-Z.; Chen, L.-H.; Li, Y.; Yang, X.-Y., Yuan, Z.-Y.; Su, B.-L. Applications of hierarchically structured porous materials from energy storage and conversion, catalysis, photocatalysis, adsorption, separation, and sensing to biomedicine. *Chem. Soc. Rev.* **2016**, *45*, 3479-3563.

(3) Pérez-Ramírez, J.; Christensen, C. H.; Egeblad K.; Christensen, C. H.; Groen, J. C. Hierarchical zeolites: enhanced utilisation of microporous crystals in catalysis by advances in materials design. *Chem. Soc. Rev.* **2008**, *37*, 2530-2542.

(4) Hartmann, M. Hierarchical zeolites: a proven strategy to combine shape selectivity with efficient mass transport. *Angew. Chem. Int. Ed.* **2004**, *43*, 5880-5882.

(5) Schwieger, W.; Machoke, A. G.; Weissenberger, T.; Inayat, A.; Selvam, T.; Klumpp, M.; Inayat, A. Hierarchy concepts: classification and preparation strategies for zeolite containing materials with hierarchical porosity. *Chem. Soc. Rev.* **2016**, *45*, 3353-3376.

(6) Lopez-Orozco, S.; Inayat, A; Schwab, A.; Selvam, T.; Schwieger, W. Zeolitic Materials with Hierarchical Porous Structures. *Adv. Mater.* **2011**, *23*, 2602-2615.

(7) Hartmann, M.; Gonche-Machoke, A.; Schwieger, W. Catalytic test reactions for the evaluation of hierarchical zeolites. *Chem. Soc. Rev.* **2016**, *45*, 3313-3330.

(8) Serrano, D. P.; Escola, J. M.; Pizarro, P. Synthesis strategies in the search for hierarchical zeolites. *Chem. Soc. Rev.* **2013**, *42*, 4004-4035.

(9) Cychosz, K. A.; Guillet-Nicolas, R.; García-Martínez, J.; Thommes, M. Recent advances in the textural characterization of hierarchically structured nanoporous materials. *Chem. Soc. Rev.* **2017**, *46*, 389-414.

(10) Verboekend, D.; Nuttens, N.; Locus, R.; Van Aelst, J.; Verolme, P.; Groen, J. C.; Pérez-Ramírez, J. Sels, B. F. Synthesis, characterisation, and catalytic evaluation of hierarchical faujasite zeolites: milestones, challenges, and future directions. *Chem. Soc. Rev.* **2016**, *45*, 3331-3352.

(11) Wei, Y.; Parmentier, T. E., de Jong, K. P.; Zečević, J. Tailoring and visualizing the pore architecture of hierarchical zeolites. *Chem. Soc. Rev.* **2015**, *44*, 7234-7261.

(12) Linares, N.; Cirujano, F. G.; De Vos, D. E.; Garcia-Martinez, J. Surfactant-templated zeolites for the production of active pharmaceutical intermediates. *Chem. Commun*. **2019**, *55*, 12869-12872.

(13) Valtchev, V.; Tosheva, L. Porous Nanosized Particles: Preparation, Properties, and Applications. *Chem. Rev.* **2013**, *113*, 6734-6760.

(14) Jiang, J.; Zhao, Y.; Yaghi, O. M. Covalent Chemistry beyond Molecules. *J. Am. Chem. Soc.* **2016**, *138*, 3255-3265.

(15) Yaghi, O. M.; O'Keeffe, M. Ockwig, N. W.; Chae, H. K.; Eddaoudi, M.; Kim, J. Reticular synthesis and the design of new materials. *Nature* **2003**, *423*, 705-714.

(16) Zhou, H.-C.; Kitagawa, S., Metal–Organic Frameworks (MOFs). *Chem. Soc. Rev.*, **2014**, *43*, 5415-5418.

(17) Cirujano, F. G.; Stalpaert, M.; De Vos, D. E. Ionic liquids vs. microporous solids as reusable reaction media for the catalytic C–H functionalization of indoles with alcohols. *Green Chem.* **2018**, *20*, 2481-2485.

(18) Cirujano, F. G. Engineered MOFs and Enzymes for the Synthesis of Active Pharmaceutical Ingredients. *ChemCatChem* **2019**, *11*, 5671-5685.

(19) Martin, N.; Cirujano, F. G. Organic synthesis of high added value molecules with MOF catalysts. *Org. Biomol. Chem.* **2020**, Accepted Manuscript, doi.org/10.1039/D0OB01571G.

(20) Férey, G.; Mellot-Draznieks, C.; Serre, C.; Millange, F.; Dutour, J.; Surblé, S.; Margiolaki, I. A Chromium Terephthalate-Based Solid with Unusually Large Pore Volumes and Surface Area. *Science* **2005**, *309*, 2040-2042.

(21) Férey, G.; Serre, C.; Mellot-Draznieks, C.; Millange, F.; Surblé, S.; Dutour, J.; Margiolaki, I. A hybrid solid with giant pores prepared by a combination of targeted chemistry, simulation, and powder diffraction. *Angew. Chem. Int. Ed.* **2004**, *43*, 6296-6301.

(22) Bhattacharjee, S.; Chen, C.; Ahn, W.-S. Chromium terephthalate metal–organic framework MIL-101: synthesis, functionalization, and applications for adsorption and catalysis. *RSC Adv.* **2014**, *4*, 52500-52525.

(23) Kholdeeva, O. A. Liquid-phase selective oxidation catalysis with metal-organic frameworks. *Catal. Today* **2016**, *278*, 22-29.

(24) Lee, Y.-R.; Yu, K.; Ravi, S.; Ahn, W.-S. Selective Adsorption of Rare Earth Elements over Functionalized Cr-MIL-101. *ACS Appl. Mater. Interfaces* **2018**, *10*, 23918-23927.

(25) Khan, N. A.; Yoo, D. K.; Jhung, S. H. Polyaniline-Encapsulated Metal–Organic Framework MIL-101: Adsorbent with Record-High Adsorption Capacity for the Removal of Both Basic Quinoline and Neutral Indole from Liquid Fuel. *ACS Appl. Mater. Interfaces* **2018**, *10*, 35639-35646.

(26) Santiago-Portillo, A. Navalon, S.; Cirujano, F. G.; Llabres i Xamena, F. X.; Alvaro, M.; Garcia, H. MIL-101 as Reusable Solid Catalyst for Autoxidation of Benzylic Hydrocarbons in the Absence of Additional Oxidizing Reagents. *ACS Catal.* **2015**, *5*, 3216-3224.

(27) Buru, C. T.; Farha, O. K. Strategies for Incorporating Catalytically Active Polyoxometalates in Metal–Organic Frameworks for Organic Transformations. *ACS Appl. Mater. Interfaces* **2020**, *12*, 5345-5360.

(28) Maksimchuk, N. V.; Kovalenko, K. A.; Arzumanov, S. S.; Chesalov, Y. A.; Melgunov, M. S.; Stepanov, A. G.; Fedin, V. P.; Kholdeeva, O. A. Hybrid polyoxotungstate/MIL-101 materials: synthesis, characterization, and catalysis of H2O2-based alkene epoxidation. *Inorg. Chem.* **2010**, *49*, 2920-2930.

(29) Juan-Alcañiz, J.; Ramos-Fernandez, E. V.; Lafont, U.; Gascon, J.; Kapteijn, F. Building MOF bottles around phosphotungstic acid ships: One-pot synthesis of bi-functional polyoxometalate-MIL-101 catalysts. *J. Catal.* **2010**, *269*, 229-241.

(30) Zhang, Y.; Degirmenci, V.; Li, C.; Hensen, E. J. M. Phosphotungstic acid encapsulated in metal-organic framework as catalysts for carbohydrate dehydration to 5-hydroxymethylfurfural. *ChemSusChem* **2010**, *4*, 59-64.

(31) Bromberg, L.; Diao, Y.; Wu, H.; Speakman, S. A.; Hatton, T. A. Chromium(III) Terephthalate Metal Organic Framework (MIL-101): HF-Free Synthesis, Structure, Polyoxometalate Composites, and Catalytic Properties. *Chem. Mater.* **2012**, *24*, 1664-1675.

(32) Wee, L. H.; Bonino, F.; Lamberti, C.; Bordiga, S.; Martens, J. A. Cr-MIL-101 encapsulated Keggin phosphotungstic acid as active nanomaterial for catalysing the alcoholysis of styrene oxide. *Green Chem.* **2014**, *16*, 1351-1357.

(33) Deng, Q.; Nie, G.; Pan, L.; Zou, J. J.; Zhang, X.; Wang, L. Highly selective self-condensation of cyclic ketones using MOF-encapsulating phosphotungstic acid for renewable high-density fuel. *Green Chem.* **2015**, *17*, 4473-4481.

(34) Wang, Y.; Zhang, Y.; Jiang, Z.; Jiang, G.; Zhao, Z.; Wu, Q.; Liu, Y.; Xu, Q.; Duan, A.; Xu, C. Controlled fabrication and enhanced visible-light photocatalytic hydrogen production of Au@CdS/MIL-101 heterostructure. *Appl. Catal. B: Environ.* **2016**, *185*, 307-314.

(35) Wen, M.; Kuwahara, Y.; Mori, K.; Zhang, D.; Li, H.; Yamashita, H. Synthesis of Ce ions doped metal–organic framework for promoting catalytic H2 production from ammonia borane under visible light irradiation. *J. Mater. Chem. A* **2015**, *3*, 14134-14141.

(36) Guo, Q.; Ren, L.; Kumar, P.; Cybulskis, V. J.; Mkhoyan, K. A.; Davis, M. E.; Tsapatsis, M. A. Chromium Hydroxide/MIL-101(Cr) Composite Catalyst and its Use for Selective Glucose Isomerization to Fructose. *Angew. Chem.* **2018**, *130*, 5020-5024.

(37) Fu, G.; Cirujano, F. G.; Krajnc, A.; Mali, G.; Henrion, M.; Smolders, S.; De Vos, D. Unexpected linker-dependent Brønsted acidity in the (Zr)UiO-66 metal organic framework and application to biomass valorization. *Catal. Sci. Technol*. **2020**,*10*, 4002-4009.

(38) Park, D.; Dinca, M.; Roman-Leshkov, Y. Heterogeneous Epoxide Carbonylation by Cooperative Ion-Pair Catalysis in Co(CO)4−-Incorporated Cr-MIL-101. *ACS Cent. Sci.* **2017**, *3*, 444-448.

(39) Eddaoudi, M.; Kim, J.; Rosi, N.; Vodak, D.; Wachter, J.; O'Keeffe, M.; Yaghi, O. M. Systematic Design of Pore Size and Functionality in Isoreticular MOFs and Their Application in Methane Storage. *Science* **2002**, *295*, 469-472.

(40) Furukawa, H.; Ko, N.; Go, Y. B.; Aratani, N.; Choi, S. B.; Choi, E.; Yazaydin, A. Ö.; Snurr, R. Q.; O'Keeffe, M.; Kim, J.; Yaghi, O. M. Ultrahigh Porosity in Metal-Organic Frameworks. *Science* **2010**, *329*, 424-428.

(41) Schaate, A.; Roy, P; Preuße, T.; Lohmeie, S. J.; Godt, A.; Behrens; P. Porous Interpenetrated Zirconium–Organic Frameworks (PIZOFs): A Chemically Versatile Family of Metal–Organic Frameworks. *Chem. Eur. J.* **2011**, *17*, 9320-9325.

(42) Lippke, J.; Brosent, B.; von Zons, T.; Virmani, E.; Lilienthal, S.; Preuße, T.; Hülsmann, M.; Schneider, A. M.; Wuttke, S.; Behrens, P.; Godt, A. Expanding the Group of Porous Interpenetrated Zr-

Organic Frameworks (PIZOFs) with Linkers of Different Lengths. *Inorg. Chem.* **2017**, *56*, 748-761.

(43) Li, P; Modica, J. A.; Howarth, A. J.; Vargas, E.; Moghadam, P. Z.; Snurr, R. Q.; Mrksich, M.; Hupp, J. T.; Farha, O. K. Toward Design Rules for Enzyme Immobilization in Hierarchical Mesoporous Metal-Organic Frameworks. *Chem* **2016**, *1*, 154-169.

(44) Mondloch, J. E. ;Bury, W. ; Fairen-Jimenez, D.; Kwon, S.; DeMarco, E. J. ; Weston, M. H. ; Sarjeant, A. A. ; Nguyen, S. B. T. ; Stair, P. C. ; Snurr, R. Q. ; Farha, O. K.; Hupp, J. T. Vapor-Phase Metalation by Atomic Layer Deposition in a Metal–Organic Framework. *J. Am. Chem. Soc.* **2013**, *135*, 10294-10297.

(45) Chen, Y.; Li, P.; Modica, J. A.; Drout, R. J.; Farha, O. K. Acid-Resistant Mesoporous Metal–Organic Framework toward Oral Insulin Delivery: Protein Encapsulation, Protection, and Release. *J. Am. Chem. Soc.* **2018**, *140*, 5678-5681.

(46) Wang, S.; Chen, Y.; Wang, S.; Li, P.; Mirkin, C. A.; Farha, O. K. DNA-Functionalized Metal–Organic Framework Nanoparticles for Intracellular Delivery of Proteins. *J. Am. Chem. Soc.* **2019**, *141*, 2215-2219.

(47) Liang, J.; Liang, K. Biocatalytic Metal-Organic Frameworks: Biocatalytic Metal–Organic Frameworks: Prospects Beyond Bioprotective Porous Matrices. *Adv. Funct. Mater.* **2020**, *30*, 2001648.

(48) Li, P.; Chen, Q.; Wang, T. C.; Vermeulen, N. A.; Mehdi, B. L.; Dohnalkova, A.; Browning, N. D.; Shen, D.; Anderson, R.; Gómez-Gualdrón, D. A.; Cetin, F. M.; Jagiello, J.; Asiri, A. M.; Fraser Stoddart, J. Farha, O. K. Hierarchically Engineered Mesoporous Metal-Organic Frameworks toward Cell-free Immobilized Enzyme Systems. *Chem* **2018**, *4*, 1022–1034.

(49) Wang, K.; Feng, D.; Liu, T. F.; Su, J.; Yuan, S.; Chen, Y. P.; Bosch, M.; Zou, X.; Zhou, H. C. A Series of Highly Stable Mesoporous Metalloporphyrin Fe-MOFs. *J. Am. Chem. Soc.* **2014**, *136*, 13983-13986.

(50) Feng, D.; Gu, Z. Y.; Li, J. R.; Jiang, H. L.; Wei, Z.; Zhou, H. C. Zirconium-Metalloporphyrin PCN-222: Mesoporous Metal–Organic Frameworks with Ultrahigh Stability as Biomimetic Catalysts. *Angew. Chem. Int. Ed.* **2012**, *124*, 10453-10456.

(51) Liu, T. F.; Feng, D.; Chen, Y. P.; Zou, L.; Bosch, M.; Yuan, S.; Wei, Z.; Fordham, S.; Wang, K.; Zhou. H. C. Topology-Guided Design and Syntheses of Highly Stable Mesoporous Porphyrinic Zirconium Metal–Organic Frameworks with High Surface Area. *J. Am. Chem. Soc.* **2015**, *137*, 413-419.

(52) Epp, K.; Bueken, B.; Hofmann, B. J.; Cokoja, M.; Hemmer, K.; De Vos, D.; Fischer, R. A. Network topology and cavity confinement-controlled diastereoselectivity in cyclopropanation reactions catalyzed by porphyrin-based MOFs. *Catal. Sci. Technol.* **2019**, *9*, 6452-6459.

(53) AlKaabi, K.; Wade, C. R.; Dincă, M. Transparent-to-Dark Electrochromic Behavior in Naphthalene-Diimide-Based Mesoporous MOF-74 Analogs. *Chem* **2016**, *1*, 264-272.

(54) Park, S. S.; Hendon, C. H.; Fielding, A. J.; Walsh, A.; O'Keeffe, M.; Dinca, M. The Organic Secondary Building Unit: Strong Intermolecular π Interactions Define Topology in MIT-25, a Mesoporous MOF with Proton-Replete Channels. *J. Am. Chem. Soc.* **2017**, *139*, 3619-3622.

(55) Krause, S.; Evans, J. D.; Bon, V.; Senkovska, I.; Iacomi, P.; Kolbe, F.; Ehrling, S.; Troschke, E.; Getzschmann, J.; Többens, D. M.; Franz, A.; Wallacher, D.; Yot, P. G.; Maurin, G.; Brunner, E.; Llewellyn, P. L.; Coudert, F. X.; Kaskel, S. Towards general network architecture design criteria for negative gas adsorption transitions in ultraporous frameworks. *Nat. Commun.* **2019**, *10*, 3632.

(56) Krause, S.; Bon, V.; Senkovska, I.; Stoeck, U.; Wallacher, D.; Többens, M.; Zander, S.; Pillai, R. S.; Maurin, G.; Coudert, F. X..; Kaskel, S. A pressure-amplifying framework material with negative gas adsorption transitions. *Nature* **2016**, *532*, 348-352.

(57) Stoeck, U.; Krause, S.; Bon, V.; Senkovska, I.; Kaskel, S. A highly porous metal–organic framework, constructed from a cuboctahedral super-molecular building block, with exceptionally high methane uptake. *Chem. Commun.* **2012**, *48*, 10841-10843.

(58) Schaber, J.; Krause, S.; Paasch, S.; Senkovska, I.; Bon, V.; Többens, D. M.; Wallacher, D.; Kaskel, S.; Brunner, E. In Situ Monitoring of Unique Switching Transitions in the Pressure-Amplifying Flexible Framework Material DUT-49 by High-Pressure 129Xe NMR Spectroscopy. *J. Phys. Chem. C* **2017**, *121*, 5195-5200.

(59) Kolbe, F.; Krause, S.; Bon, V.; Senkovska, I.; Kaskel, S.; Brunner, E. High-Pressure in Situ 129Xe NMR Spectroscopy: Insights into Switching Mechanisms of Flexible Metal–Organic Frameworks Isoreticular to DUT-49. *Chem. Mater.* **2019**, *31*, 6193-6201.

(60) Forse, A. C.; Colwell, K. A.; Gonzalez, M. I.; Benders, S.; Torres-Gavosto, R. M.; Blümich, B.; Reimer, J. A.; Long; J. R. Influence of Pore Size on Carbon Dioxide Diffusion in Two Isoreticular Metal–Organic Frameworks. *Chem. Mater.* **2020**, *32*, 3570-3576.

(61) Feng, D.; Wang, K.; Su, J; Liu, T. F.; Park, J.; Wei, Z.; Bosch, M.; Yakovenko, A.; Zou, X; Zhou H.-C. A Highly Stable Zeotype Mesoporous Zirconium Metal–Organic Framework with Ultralarge Pores. *Angew. Chem. Int. Ed.* **2015**, *54,* 149-154.

(62) Navarro, J. A. R. Impact of Defects on Pyrazolate Based Metal Organic Frameworks. *Isr. J. Chem.* **2018**, *58*, 1112-1118.

(63) Colombo, V.; Montoro, C.; Maspero, A.; Palmisano, G.; Masciocchi, N.; Galli, S.; Barea, E.; Navarro, J. A. R. Tuning the Adsorption Properties of Isoreticular Pyrazolate-Based Metal–Organic Frameworks through Ligand Modification. *J. Am. Chem. Soc.* **2012**, *134*, 12830-12843.

(64) Cirujano, F. G.; Lopez-Maya, E.; Rodriguez-Albelo, M.; Barea, E.; Navarro, J. A. R.; De Vos, D. E. Selective One-Pot Two-Step C–C Bond Formation using Metal–Organic Frameworks with Mild Basicity as Heterogeneous Catalysts. *ChemCatChem*. **2017**, *9*, 4019-4023.

(65) Cirujano, F. G.; López-Maya, E.; Navarro, J. A. R.; De Vos, D. E. Pd(II)-Ni(II) pyrazolate framework as active and recyclable catalyst for the hydroamination of terminal alkynes. *Top. Catal.* **2018**, *61*, 1414-1423.

(66) Park, S. S.; Tulchinsky, Y.; Dinca, M. Single-Ion Li+, Na+, and Mg2+ Solid Electrolytes Supported by a Mesoporous Anionic Cu–Azolate Metal–Organic Framework. *J. Am. Chem. Soc.* **2017**, *139*, 13260-13263.

(67) Fang, Z.; Bueken, B.; De Vos, D. E; Fischer, R. A. Defect-Engineered Metal-Organic Frameworks. *Angew. Chem. Int. Ed.* **2015**, *54*, 7234-7254.

(68) Cheetham, A. K.; Bennett, T. D.; Coudert, F. X.; Goodwin, A. L. Defects and disorder in metal organic frameworks. *Dalton Trans.*, **2016**, *45*, 4113-4126.

(69) Dissegna, S.; Epp, K..; Heinz, W. R.; Kieslich, G.; Fischer, R. A. Defective Metal-Organic Frameworks, *Adv. Mater.* **2018**, *30*, 1704501.

(70) Koh, K.; Wong-Foy, A. G.; Matzger, A. J. A crystalline mesoporous coordination copolymer with high microporosity. *Angew. Chem. Int. Ed.* **2008**, *47*, 677-680.

(71) K Koh, K.; Wong-Foy, A. G.; Matzger, A. J. A Porous Coordination Copolymer with over 5000 m2/g BET Surface Area. *J. Am. Chem. Soc.* **2009**, *131*, 4184-4185.

(72) Babu, R.; Kathalikkattil, A. C.; Roshan, R.; Tharun, J.; Kim, D.-W.; Park, D.-W. Dual-porous metal organic framework for room temperature CO2 fixation via cyclic carbonate synthesis. *Green Chem.* **2016**, *18*, 232-242.

(73) Wang, Z.; Tanabe, K. K.; Cohen, S. M. Accessing Postsynthetic Modification in a Series of Metal-Organic Frameworks and the Influence of Framework Topology on Reactivity. *Inorg. Chem.* **2009**, *48*, 296-306.

(74) Tanabe, K. K.; Cohen, S. M. Engineering a metal-organic framework catalyst by using postsynthetic modification. *Angew. Chem. Int. Ed.* **2009**, *48*, 7424-7427.

(75) Tanabe, K. K.; Cohen, S. M. Postsynthetic modification of metal–organic frameworks—a progress report. *Chem. Soc. Rev.* **2011**, *40*, 498–519.

(76) Klein, N.; Senkovska, I.; Gedrich, K.; Stoeck, U.; Henschel, A.; Mueller, U.; Kaskel, S. A Mesoporous Metal–Organic Framework. *Angew. Chem. Int. Ed.* **2009**, *48*, 9954-9957.

(77) Grünker, R.; Bon, V.; Müller, P.; Stoeck, U.; Krause, S.; Mueller, U.; Senkovska, I.; Kaskel, S. A new metal–organic framework with ultra-high surface area. *Chem. Commun.* **2014**, *50*, 3450-3452.

(78) Furukawa, H.; Ko, N.; Go, Y. B.; Aratani, S. B.; Choi, S. B.; Choi, E.; Yazaydin, A. Ö.; Snurr, R. Q.; O'Keeffe, M.; Kim, J.; Yaghi, O. M. Ultrahigh Porosity in Metal-Organic Frameworks. *Science* **2010**, *329*, 424-428.

(79) Hönicke, I. M.; Senkovska, I.; Bon, V.; Baburin, I. A.; Bönisch, N.; Raschke, S.; Evans, J. D.; Kaskel, S. Balancing Mechanical Stability and Ultrahigh Porosity in Crystalline Framework Materials. *Angew. Chem. Int. Ed.* **2018**, *57*, 13780-13783.

(80) Wang, Z.; Henke, S.; Paulus, M.; Welle, A.; Fan, Z.; Rodewald, K.; Rieger, B.; Fischer, R. A. Defect Creation in Surface-Mounted Metal–Organic Framework Thin Films. *ACS Appl. Mater. Interfaces* **2020**, *12*, 2655–2661.

(81) Kozachuk, O.; Luz, I.; Llabrés i Xamena, F. X.; Noei, H.; Kauer, M.; Bauke-Albada, H.; Bloch, E. D.; Marler, B.; Wang, Y.; Muhler, M.; Fischer, R. A. Multifunctional, Defect-Engineered Metal–Organic Frameworks with Ruthenium Centers: Sorption and Catalytic Properties. *Angew. Chem. Int. Ed.* **2014**, *53*, 7058-7062.

(82) Zhang, W.; Kauer, M.; Halbherr, O.; Epp, K.; Guo, P.; Gonzalez, M. I.; Xiao, D. J.; Wiktor, C.; LIabrés i Xamena, F. X.; Wöll, C.; Wang, Y.; Muhler, M.; Fischer, R. A. Ruthenium Metal–Organic Frameworks with Different Defect Types: Influence on Porosity, Sorption, and Catalytic Properties *Chem. Eur. J.* **2016**, *22*, 14297-14307.

(83) Epp, K.; Luz, I.; Heinz, W. R.; Rapeyko, A.; Llabrés i Xamena, F. X.; Fischer, R. A. Defect-Engineered Ruthenium MOFs as Versatile Heterogeneous Hydrogenation Catalysts. *ChemCatChem* **2020**, *12*, 1720-1725.

(84) Nickerl, G.; Stoeck, U.; Burkhardt, U.; Senkovska, I. Kaskel, S. A catalytically active porous coordination polymer based on a dinuclear rhodium paddle-wheel unit. *J. Mater. Chem. A*, **2014**, *2*, 144-148.

(85) Fang, Z.; Dürholt, J. P.; Kauer, M.; Zhang, W.; Lochenie, C.; Jee, B.; Albada, B.; Metzler-Nolte, N.; Pöppl, A.; Weber, B.; Muhler, M.; Wang, Y.; Schmid, R.; Fischer, R. A. Structural Complexity in Metal–Organic Frameworks: Simultaneous Modification of Open Metal Sites and Hierarchical Porosity by Systematic Doping with Defective Linkers. *J. Am. Chem. Soc.* **2014**, *136*, 9627–9636.

(86) Dissegna, S.; Hardian, R.; Epp, K.; Kieslich, G.; Coulet, M. V.; Llewellyn, P.; Fischer, R. A. Using water adsorption measurements to access the chemistry of defects in the metal–organic framework UiO-66. *CrystEngComm*, **2017**, *19*, 4137-4141.

(87) Dissegna, S.; Vervoorts, P.; Hobday, C. L.; Düren, T.; Daisenberger, D.; Smith, A. J.; Fischer, R. A.; Kieslich, G. Tuning the Mechanical Response of Metal–Organic Frameworks by Defect Engineering. *J. Am. Chem. Soc.* **2018**, *140*, 11581-11584.

(88) Vermoortele, F.; Bueken, B.; Le Bars, G.; Van de Voorde, B.; Vandichel, M.; Houthoofd, K.; Vimont, A.; Daturi, M.; Waroquier, M.; Van Speybroeck, V.; Kirschhock, C.; De Vos, D. E. Synthesis Modulation as a Tool To Increase the Catalytic Activity of Metal–Organic Frameworks: The Unique Case of UiO-66(Zr). *J. Am. Chem. Soc.* **2013**, *135*, 11465–11468.

(89) Van de Voorde, B.; Stassen, I.; Bueken, B.; Vermoortele, F.; De Vos, D.; Ameloot, R.; Tan, J. C.; Bennett, T. D. Improving the mechanical stability of zirconium-based metal–organic frameworks by incorporation of acidic modulators. *J. Mater. Chem. A* **2015**, *3*, 1737-1742.

(90) Diring, S.; Furukawa, S.; Takashima, Y.; Tsuruoka, T.; Kitagawa, S. Controlled Multiscale Synthesis of Porous Coordination Polymer in Nano/Micro Regimes. *Chem. Mater.* **2010**, 22, 4531–4538.

(91) Kozachuk, O.; Yusenko, K.; Noei, H.; Wang, Y.; Walleck, S.; Glaserc, T.; Fischer, R. A. Solvothermal growth of a ruthenium metal–organic framework featuring HKUST-1 structure type as thin films on oxide surfaces. *Chem. Commun.* **2011**, *47*, 8509-8511.

(92) Heinz, W. R.; Kratky, T.; Drees, M.; Wimmer, A.; Tomanec, O.; Günther, S.; Schuster, M; Fischer, R. A. Mixed precious-group metal–organic frameworks: a case study of the HKUST-1 analogue [RuxRh3−x(BTC)2]. *Dalton Trans.* **2019**, *48,* 12031-12039.

(93) Cai, G.; Jiang, H. L. A Modulator-Induced Defect-Formation Strategy to Hierarchically Porous Metal-Organic Frameworks with High Stability. *Angew. Chem. Int. Ed.* **2017**, *56*, 563-567.

(94) Park, J.; Wang, Z. U.; Sun, L. B.; Chen, Y. P.; Zhou, H. C. Introduction of Functionalized Mesopores to Metal–Organic Frameworks via Metal–Ligand–Fragment Coassembly. *J. Am. Chem. Soc.* **2012**, *134*, 20110-20116.

(95) Wang, C. C.; Yang, C. C.; Yeh, C. T.; Cheng, K. Y.; Chang, P. C.; Ho, M. L.; Lee, G. H.; Shih, W. J.; Sheu, H. S. Reversible solid-state structural transformation of a 1D-2D coordination polymer by thermal De/rehydration processes. *Inorg. Chem.* **2011**, *50*, 597-603.

(96) Lee, S. C.; Choi, E. Y.; Lee, S. B.; Kim, S. W.; Kwon, O. P. Unusual Transformation from a Solvent-Stabilized 1D Coordination Polymer to a Metal–Organic Framework (MOF)-Like Cross-Linked 3D Coordination Polymer. *Chem. Eur. J.* **2015**, *21*, 15570-15574.

(97) Wen, L.; Cheng, P.; Lin, W. Solvent-induced single-crystal to single-crystal transformation of a 2D coordination network to a 3D metal–organic framework greatly enhances porosity and hydrogen uptake. *Chem. Commun.* **2012**, *48*, 2846-2848.

(98) Liu, D.; Ren, Z. G.; Li, H. X.; Lang, J. P.; Li, N. Y.; Abrahams, B. F. Single-Crystal-to-Single-Crystal Transformations of Two Three-Dimensional Coordination Polymers through Regioselective [2+2] Photodimerization Reactions. *Angew. Chem. Int. Ed.* **2010**, *49*, 4767-4770.

(99) Bennett, T. D.; Cheetham, A. K. Amorphous Metal–Organic Frameworks. *Acc. Chem. Res.* **2014**, *47, 5*, 1555-1562.

(100) Katsenis, A. D.; Puškarić, A.; Štrukil, V.; Mottillo, C.; Julien, P. A.; Užarević, K.; Pham, M. H.; Do, T. O.; Kimber, S. A. J.; Lazić, P.; Magdysyuk, O.; Dinnebier, R. E.; Halasz, I.; Friščić, T. In situ X-ray diffraction monitoring of a mechanochemical reaction reveals a unique topology metal-organic framework. *Nat. Commun.* **2015**, *6*, 6662.

(101) Cao, S.; Bennett, T. D.; Keen, D. A.; Goodwin, A. L.; Cheetham, A. K. Amorphization of the prototypical zeolitic imidazolate framework ZIF-8 by ball-milling. *Chem. Commun.* **2012**, *48*, 7805-7807.

(102) Wee, L. H.; Meledina, M.; Turner, S.; Van Tendeloo, G.; Zhang, K.; Rodriguez-Albelo, M. L.; Masala, A.; Bordiga, S.; Jiang, J.; Navarro, J. A. R.; Kirschhock, C. E. A.; Martens, J. A. 1D-2D-3D Transformation Synthesis of Hierarchical Metal–Organic Framework Adsorbent for Multicomponent Alkane Separation. *J. Am. Chem. Soc.* **2017**, *139*, 819-828.

(103) Roy, X.; MacLachlan, M. J. Coordination Chemistry: New Routes to Mesostructured Materials. *Chem. Eur. J.* **2009**, *15*, 6552-6559.

(104) Bradshaw, D.; El-Hankari, S.; Lupica-Spagnolo, L. Supramolecular templating of hierarchically porous metal–organic frameworks. *Chem. Soc. Rev.* **2014**, *43*, 5431-5443.

(105) Seoane, B.; Castellanos, S.; Dikhtiarenko, A.; Kapteijn, F.; Gascon, J. Multi-scale crystal engineering of metal organic frameworks. *Coord. Chem. Rev.* **2016**, *307*, 147-187.

(106) Qiu, L. G.; Xu, T.; Li, Z. Q.; Wang, W.; Wu, Y.; Jiang, X.; Tian, X. Y.; Zhang, L. D. Hierarchically Micro- and Mesoporous Metal–Organic Frameworks with Tunable Porosity. *Angew. Chem. Int. Ed.* **2008**, *47*, 9487-9633.

(107) Wee, L. H.; Wiktor, C.; Turner, S.; Vanderlinden, W.; Janssens, N.; Bajpe, S. R.; Houthoofd, K.; Van Tendeloo, G.; De Feyter, S.; Kirschhock, C. E. A.; Martens, J. A. Copper Benzene Tricarboxylate Metal–Organic Framework with Wide Permanent

Mesopores Stabilized by Keggin Polyoxometallate Ions. *J. Am. Chem. Soc.* **2012**, 134, 10911-10919.

(108) Junggeburth, S. C.; Schwinghammer, K.; Virdi, K. S.; Scheu, C.; Lotsch, B. V. Towards Mesostructured Zinc Imidazolate Frameworks. *Chem. Eur. J.* **2012**, *18*, 2143-2152.

(109) Flügel, E. A.; Aronson, M. T.; Junggeburth, S. C.; Chmelkad, B. F.; Lotsch, B. V. Surfactant-directed syntheses of mesostructured zinc imidazolates: formation mechanism and structural insights. *CrystEngComm* **2015**, *17*, 463-470.

(110) Avci, C.; Imaz, I.; Carné-Sánchez, A.; Pariente, J. A.; Tasios, N.; Pérez-Carvajal, J.; Alonso, M. I.; Blanco, A.; Dijkstra, M.; López, C.; Maspoch, D. Self-assembly of polyhedral metal-organic framework particles into three-dimensional ordered superstructures. *Nat. Chem* **2018**, *10*, 78-84.

(111) El-Hankari, S.; Huo, J.; Ahmed, A.; Zhang, H.; Bradshaw, D. Surface etching of HKUST-1 promoted via supramolecular interactions for chromatography. *J. Mater. Chem. A* **2014**, *2*, 13479-13485.

(112) Kang, X.; Lyu, K.; Li, L.; Li, J.; Kimberley, L.; Wang, B.; Liu, L.; Cheng, Y.; Frogley, M. D.; Rudić, S.; Ramirez-Cuesta, A. J.; Dryfe, R. A. W.; Han, B.; Yang, S.; Schröder, M. Integration of mesopores and crystal defects in metal-organic frameworks via templated electrosynthesis. *Nat. Commun*. **2019**, *10*, 4466.

(113) Li, K.; Yang, J.; Huang, R.; Lin, S.; Gu, J. Ordered Large-Pore MesoMOFs Based on Synergistic Effects of TriBlock Polymer and Hofmeister Ion. *Angew. Chem.* **2020**, *132*, 14228-14232.

(114) Cirujano, F. G.; Luz, I.; Soukri, I.; Van Goethem, C.; Vankelecom, I. F. J.; Lail, M.; De Vos, D. E. Boosting the Catalytic Performance of Metal–Organic Frameworks for Steroid Transformations by Confinement within a Mesoporous Scaffold. *Angew. Chem. Int. Ed.* **2017**, *56*, 13302-13306.

(115) Marquez, C.; Rivera-Torrente, M.; Paalanen, P. P.; Weckhuysen, B. M; Cirujano, F. G.; De Vos, D.; De Baerdemaeker, T. Increasing the availability of active sites in Zn-Co double metal cyanides by dispersion onto a SiO2 support. *J. Catal.* **2017**, *354*, 92-99.

(116) Martín, N.; Portillo, A.; Ateka, A.; Cirujano, F. G.; Oar-Arteta, L.; Aguayo, A. T.; Dusselier, M. MOF-derived/zeolite hybrid catalyst for the production of light olefins from CO2. *ChemCatChem* **2020**, Accepted Manuscript, doi.org/10.1002/cctc.202001109.

(117) Choi, K. M.; Jeon, H. J.; Kang, J. K.; Yaghi, O. M. Heterogeneity within Order in Crystals of a Porous Metal–Organic Framework. *J. Am. Chem. Soc.* **2011**, *133*, 11920-11923.

(118) He, S.; Chen, Y.; Zhang, Z.; Ni, B.; He, W.; Wang, X. Competitive coordination strategy for the synthesis of hierarchical-pore metal–organic framework nanostructures. *Chem. Sci.* **2016**, *7*, 7101-7105.

(119) Cirujano, F. G. MOFs vs. zeolites: carbonyl activation with M(IV) catalytic sites. *Catal. Sci. Technol.* **2017**, *7*, 5482-5494.

(120) Cirujano, F. G; Llabrés i Xamena, F. X. Tuning the Catalytic Properties of UiO-66 Metal–Organic Frameworks: From Lewis to Defect-Induced Brønsted Acidity. *J. Phys. Chem. Lett.* **2020**, *11*, 4879-4890.

(121) Valenzano, L.; Civalleri, B.; Chavan, S.; Bordiga, S.; Nilsen, M. H.; Jakobsen, S.; Lillerud, K. P.; Lamberti. C. Disclosing the Complex Structure of UiO-66 Metal Organic Framework: A Synergic Combination of Experiment and Theory. *Chem. Mater.* **2011**, *23*, 1700-1718.

(122) Shearer, G. C.; Chavan, S.; Ethiraj, J.; Vitillo, J. G.; Svelle, S.; Olsbye, U.; Lamberti, C.; Bordiga, S.; Lillerud, K. P. Tuned to Perfection: Ironing Out the Defects in Metal–Organic Framework UiO-66. *Chem. Mater.* **2014**, *26*, 4068-4071.

(123) Shearer, G. C.; Chavan, S.; Bordiga, S.; Svelle, S.; Olsbye, U.; Lillerud, K. P. Defect Engineering: Tuning the Porosity and Composition of the Metal–Organic Framework UiO-66 via Modulated Synthesis. *Chem. Mater.* **2016**, *28*, 3749-3761.

(124) Lupica-Spagnolo, L.; Ward, D. J.; Marie, J. J.; Lymperopouloua, S.; Bradshaw, D. Pollen-like ZIF-8 colloidosomes via emulsion templating and etching. *Chem. Commun.* **2018**, *54*, 8506-8509.

(125) Cheng, K.; Svec, F.; Lv, Y.; Tan, T. Hierarchical Micro- and Mesoporous Zn-Based Metal-Organic Frameworks Templated by Hydrogels: Their Use for Enzyme Immobilization and Catalysis of Knoevenagel Reaction. *Small* **2019**, 1902927.

(126) Chen, C.; Zhu, H.; Li, B. G.; Zhu, S. Structuring Metal–Organic Framework Materials into Hierarchically Porous Composites through One-Pot Fabrication Strategy. *Chem. Eur. J.* **2020**, *26*, 3358-3363.

(127) Shen, K.; Zhang, L.; Chen, X.; Liu, L.; Zhang, D.; Han, Y.; Chen, J.; Long, J.; Luque, R.; Li, Y.; Chen, B. Ordered macro-microporous metal-organic framework single crystals. *Science* **2018**, *359*, 206-210.

(128) Dutta, S.; Kumari, N.; Dubbu, S.; Jang, S. W.; Kumar, A.; Ohtsu, H.; Kim, J.; Cho, S. H.; Kawano, M.; Lee, I. S. Highly Mesoporous Metal-Organic Frameworks as Synergistic Multimodal Catalytic Platforms for Divergent Cascade Reactions. *Angew. Chem. Int. Ed.* **2020**, *59*, 3416-3422.

(129) Hu, Y.; Xu, X.; Zheng, B.; Hou, S.; Wang, P.; Chen, W.; Gao, C.; Gu, Z.; Shen, Y.; Wu, J.; Fu, Y.; Zhang, W.; Huo, F. Functional Macro-Microporous Metal–Organic Frameworks for Improving the Catalytic Performance. *Small Methods* **2019**, 1800547.

(130) Meng, F.; Zhang, S.; Ma, L.; Zhang, W.; Li, M.; Wu, T.; Li, H.; Zhang, T.; Lu, X.; Huo, F.; Lu, J. Construction of Hierarchically Porous Nanoparticles@Metal–Organic Frameworks Composites by Inherent Defects for the Enhancement of Catalytic Efficiency. *Adv. Mater.* **2018**, 1803263.

(131) Xiao, Y. Y.; Liu, X. L.; Chang, G. G.; Pu, C.; Tian, G.; Wang, L. Y.; Liu, J. W.; Ma, X. C.; Yang, X. Y.; Chen, B. Construction of a functionalized hierarchical pore metal–organic framework via a palladium-reduction induced strategy. *Nanoscale* **2020**, *12*, 6250-6255.

(132) Huang, H.; Li, J. R.; Wang, K.; Han, T.; Tong, M.; Li, L.; Xie, Y.; Yang, Q.; Liu, D.; Zhong, C. An in situ self-assembly template strategy for the preparation of hierarchical-pore metal-organic frameworks. *Nat. Commun.* **2015**, *6*, 8847.

(133) Wee, L. H.; Lohe, M. R.; Janssens, N.; Kaskel, S.; Martens, J. A. Fine tuning of the metal–organic framework Cu3(BTC)2 HKUST-1 crystal size in the 100 nm to 5 micron range. *J. Mater. Chem.* **2012**, *22*, 13742-13746.

(134) Wee, L. H.; Bajpe, S. R.; Janssens, N.; Hermans, I.; Houthoofd, K.; Kirschhock, C. E. A.; Martens, J. A. Convenient synthesis of Cu3(BTC)2 encapsulated Keggin heteropolyacid nanomaterial for application in catalysis. *Chem. Commun.* **2010**, *46*, 8186-8188.

(135) Yue, Y.; Qiao, Z. A.; Fulvio, P. F.; Binder, A. J.; Tian, C.; Chen, J.; Nelson, K. M.; Zhu, X.; Dai, S. Facile Fabricating Hierarchically Porous Metal–Organic Frameworks via a Template-Free Strategy. *Cryst. Growth Des.* **2016**, *16*, 504-510.

(136) Peng, L.; Zhang, J.; Xue, Z.; Han, B.; Sang, X.; Liu, C.; Yang, G. Highly mesoporous metal–organic framework assembled in a switchable solvent. *Nat. Commun.* **2014**, *5*, 4465.

(137) Yue, Y.; Qiao, Z. A.; Fulvio, P. F.; Binder, A. J.; Tian, C.; Chen, J.; Nelson, K. M.; Zhu, X.; Dai, S. Template-Free Synthesis of Hierarchical Porous Metal–Organic Frameworks. *J. Am. Chem. Soc.* **2013**, *135*, 9572-9575.

(138) Díaz-García, M.; Mayoral, A.; Díaz, I.; Sánchez-Sánchez, M. Nanoscaled M-MOF-74 Materials Prepared at Room Temperature. *Cryst. Growth Des.* **2014**, *14*, 2479-2487.

(139) Ruano, D.; Díaz-García, M.; Alfayate, A.; Sánchez-Sánchez, M. Nanocrystalline M–MOF-74 as Heterogeneous Catalysts in the Oxidation of Cyclohexene: Correlation of the Activity and Redox Potential. *ChemCatChem* **2015**, *7*, 674-681.

(140) Cirujano, F. G.; Leo, P.; Vercammen, J.; Smolders, S.; Orcajo, G.; De Vos, D. E. MOFs Extend the Lifetime of Pd(II) Catalyst for Room Temperature Alkenylation of Enamine-Like Arenes. *Adv. Synth. Catal.* **2018**, *360*, 3872-3876.

(141) Van Velthoven, N.; Henrion, M.; Dallenes, J.; Krajnc, A.; Bugaev, A. L.; Liu, P.; Bals, S.; Soldatov, A. V.; Mali, G.; De Vos, D. E. S,O-Functionalized Metal–Organic Frameworks as Heterogeneous

Single-Site Catalysts for the Oxidative Alkenylation of Arenes via C–H activation. *ACS Catal.* **2020**, *10*, 5077-5085.

(142) Cirujano, F. G.; Martín, N.; Fu, G.; Jia, C.; De Vos, D. Cooperative acid–base bifunctional ordered porous solids in sequential multi-step reactions: MOF vs. mesoporous silica. *Catal. Sci. Technol.* **2020**, *10*, 1796-1802.

(143) Bueken, B.; Van Velthoven, N.; Willhammar, T.; Stassin, T.; I. Stassen, I.; Keen, D. A.; Baron, G. V.; Denayer, J. F. M.; Ameloot, R.; Bals, S.; De Vos, D.; Bennett, T. D. Gel-based morphological design of zirconium metal–organic frameworks. *Chem. Sci.* **2017**, *8*, 3939-3948.

(144) Connolly, B. M.; Aragones-Anglada, M.; Gandara-Loe, J.; N.; Danaf, A.; Lamb, D. C.; Mehta, J. P.; Vulpe, D.; Wuttke, S.; Silvestre-Albero, J.; Moghadam, P. Z.; Wheatley, A. E. H.; Fairen-Jimenez, D. Tuning porosity in macroscopic monolithic metal-organic frameworks for exceptional natural gas storage. *Nat. Comm.* **2019**, *10*, 2345.

(145) Zhang, W.; Kauer, M.; Guo, P.; Kunze, S.; Cwik, S.; Muhler, M.; Wang, Y.; Epp, K.; Kieslich, G.; Fischer, R. A. Impact of Synthesis Parameters on the Formation of Defects in HKUST-1. *Eur. J. Inorg. Chem.* **2017**, *2017*, 925-931.

(146) Wee, L. H.; Lescouet, T.; Ethiraj, J.; Bonino, F.; Vidruk, R.; Garrier, E.; Packet, D.; Bordiga, S.; Farrusseng, D.; Herskowitz, M.; Martens, J. A. Hierarchical Zeolitic Imidazolate Framework-8 Catalyst for Monoglyceride Synthesis. *ChemCatChem* **2013**, *5*, 3562-3566.

(147) Kim, S. Y.; Kim, A. R.; Yoon, J. W.; Kim, H. J.; Bae, Y. S. Creation of mesoporous defects in a microporous metal-organic framework by an acetic acid-fragmented linker co-assembly and its remarkable effects on methane uptake. *Chem. Eng. J.* **2018**, *335*, 94-100.

(148) Doan, H. V.; Sartbaeva, A.; Eloi, J. C.; Davis, S. A.; Ting, V. P. Defective hierarchical porous copper-based metal-organic frameworks synthesised via facile acid etching strategy. *Sci. Rep.* **2019** *9*, 10887.

(149) Koo, J.; Hwang, I. C.; Yu, X.; Saha, S.; Kim, Y.; Kim, K. Hollowing out MOFs: hierarchical micro- and mesoporous MOFs with tailorable porosity via selective acid etching. *Chem. Sci.* **2017**, *8*, 6799-6803.

(150) Yuan, S.; Zou, L.; Qin, J. S.; Li, J.; Huang, L.; Feng, L.; Wang, X.; Bosch, M.; Alsalme, A.; Cagin, T.; Zhou, H. C. Construction of hierarchically porous metal–organic frameworks through linker labilization. *Nat. Commun.* **2017**, *8*, 15356.

(151) Feng, L.; Yuan, S.; Zhang, L. L.; Tan, K.; Li, J. L.; Kirchon, A.; Liu, M.; Zhang, P.; Han, Y.; Chabal, Y. J.; Zhou, H. C. Creating Hierarchical Pores by Controlled Linker Thermolysis in Multivariate Metal–Organic Frameworks. *J. Am. Chem. Soc.* **2018**, *140*, 2363-2372.

(152) Heinz, W. R.; Agirrezabal-Telleria, I.; Junk, R.; Berger, J.; Wang, J.; Sharapa, D. I.; Gil-Calvo, M.; Luz, I.; Soukri, M.; Studt, F.; Wang, Y.; Wöll, C.; Bunzen, H.; Drees, M.; Fischer, R. A. Thermal Defect Engineering of Precious Group Metal–Organic Frameworks: A Case Study on Ru/Rh-HKUST-1 Analogues. *ACS Appl. Mater. Interfaces* **2020**, *12*, 40635-40647.

(153) Wang, K. Y.; Feng, L.; Yan, T. H.; Wu, S.; Joseph, E. A.; Zhou, H. C. Rapid Generation of Hierarchically Porous Metal-Organic Frameworks through Laser Photolysis. *Angew. Chem. Int. Ed.* **2020**, *59*, 11349-11354.

(154) Kim, Y.; Yang, T.; Yun, G.; Ghasemian, M. B.; Koo, J.; Lee, E.; Cho, S. J.; Kim, K. Hydrolytic Transformation of Microporous Metal–Organic Frameworks to Hierarchical Micro- and Mesoporous MOFs. *Angew. Chem. Int. Ed.* **2015**, *54*, 13273-13278.

(155) Tamames-Tabar, C.; Cunha, D.; Imbuluzqueta, E.; Ragon, F.; Serre, C.; Blanco-Prieto, M. J.; Horcajada, P. Cytotoxicity of nanoscaled metal–organic frameworks. *J. Mater. Chem. B* **2014**, *2*, 262-271.

(156) Feng, X.; Hajek, J.; Jena, H. S.; Wang, G.; Veerapandian, S. K. P.; Morent, R.; De Geyter, N.; Leyssens, K.; Hoffman, A. E. J.; Meynen, V.; Marquez, C.; De Vos, D. E.; Van Speybroeck, V.; Leus, K.; Van Der Voort, P. Engineering a Highly Defective Stable UiO-66 with Tunable Lewis- Brønsted Acidity: The Role of the Hemilabile Linker. *J. Am. Chem. Soc.* **2020**, *142*, 3174-3183.

(157) Martin, N.; Dusselier, M.; De Vos, D. E.; Cirujano, F. G. Metal-Organic Framework Derived Metal Oxide Clusters in Porous Aluminosilicates: A Catalyst Design for the Synthesis of Bioactive aza-Heterocycles. *ACS Catal.* **2019**, *9*, 44-48.

(158) DeSantis, D.; Mason, J. A.; James, B. D.; Houchins, C.; Long, J. R.; Veenstra, M. Techno-economic Analysis of Metal–Organic Frameworks for Hydrogen and Natural Gas Storage. *Energy Fuels* **2017**, *31*, 2024-2032.

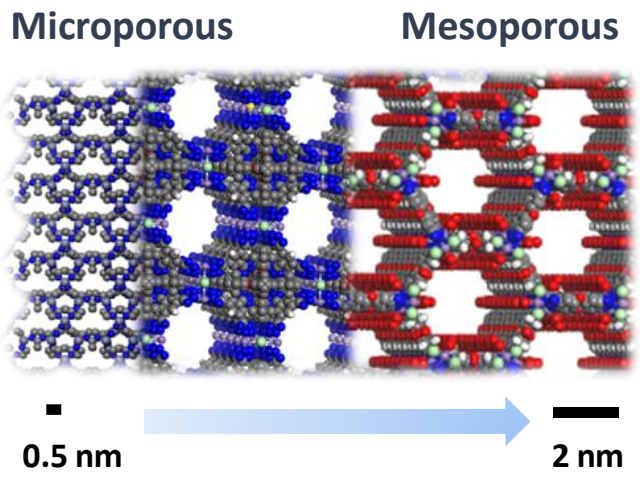

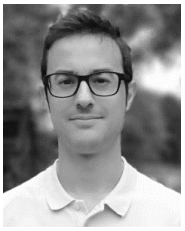

Francisco García Cirujano completed a PhD in Chemistry (2016) at the Institute of Chemical Technology and did postdoctoral stay as a Marie Curie fellow in the group of Prof. de Vos at KU-Leuven. He is now a Junior Leader La Caixa at the University of Valencia working on the design and synthesis of high performance metal-organic framework catalysts to achieve environmentally benign processes in the chemical and pharmaceutical industry

Nuria Martín García obtained a PhD in Chemistry (2017) at ITQ-UPV-CSIC. After that she moved to Belgium as a Marie Curie fellow in KU-Leuven. Her work was recognized with several prizes such as the Borealis Innovation Award and Extraordinary PhD Award. She is now a Juan de la Cierva Fellow at the University of Valencia, working on the development of sustainable catalytic processes with industrial interest and low environmental impact.

Lik Hong Wee pursued his PhD at the Manchester Metropolitan University (2008) and has been a Fonds Wetenschappelijk Onderzoek (FWO) postdoctoral research associate at the University of Leuven (2009-2019) where he has developed new protocols for the synthesis of hierarchical and nanosized metal-organic frameworks (MOFs). He is now an independent FWO senior research fellow at the University of Cambridge, working on the synthesis and processing of zeolites and MOFs for gas storage, separation and catalysis.